
Accelerated Article Preview

Fc-engineered antibody therapeutics with improved anti-SARS-CoV-2 efficacy

Received: 23 May 2021

Accepted: 13 September 2021

Accelerated Article Preview Published
online 21 September 2021

Cite this article as: Yamin, R. et al.
Fc-engineered antibody therapeutics with
improved anti-SARS-CoV-2 efficacy. *Nature*
<https://doi.org/10.1038/s41586-021-04017-w> (2021).

Rachel Yamin, Andrew T Jones, Hans-Heinrich Hoffmann, Alexandra Schäfer, Kevin S Kao, Rebecca L Francis, Timothy P Sheahan, Ralph S Baric, Charles M Rice, Jeffrey V Ravetch & Stylianos Bournazos

This is a PDF file of a peer-reviewed paper that has been accepted for publication. Although unedited, the content has been subjected to preliminary formatting. Nature is providing this early version of the typeset paper as a service to our authors and readers. The text and figures will undergo copyediting and a proof review before the paper is published in its final form. Please note that during the production process errors may be discovered which could affect the content, and all legal disclaimers apply.

Fc-engineered antibody therapeutics with improved anti-SARS-CoV-2 efficacy

<https://doi.org/10.1038/s41586-021-04017-w>

Received: 23 May 2021

Accepted: 13 September 2021

Published online: 21 September 2021

Rachel Yamin^{1,5}, Andrew T Jones^{1,5}, Hans-Heinrich Hoffmann², Alexandra Schäfer³, Kevin S Kao¹, Rebecca L Francis¹, Timothy P Sheahan³, Ralph S Baric^{3,4}, Charles M Rice², Jeffrey V Ravetch^{1,6} & Stylianos Bournazos^{1,6}

Monoclonal antibodies (mAbs) with neutralizing activity against SARS-CoV-2 have demonstrated clinical benefit in cases of mild to moderate SARS-CoV-2 infection, substantially reducing the risk for hospitalization and severe disease^{1–4}. Treatment generally requires the administration of high doses of these mAbs with limited efficacy in preventing disease complications or mortality among hospitalized COVID-19 patients⁵. Here we report the development and evaluation of Fc-optimized anti-SARS-CoV-2 mAbs with superior potency to prevent or treat COVID-19 disease. In several animal models of COVID-19 disease^{6,7}, we demonstrate that selective engagement of activating FcγRs results in improved efficacy in both preventing and treating disease-induced weight loss and mortality, significantly reducing the dose required to confer full protection upon SARS-CoV-2 challenge and treatment of pre-infected animals. Our results highlight the importance of FcγR pathways in driving antibody-mediated antiviral immunity, while excluding any pathogenic or disease-enhancing effects of FcγR engagement of anti-SARS-CoV-2 antibodies upon infection. These findings have important implications for the development of Fc-engineered mAbs with optimal Fc effector function and improved clinical efficacy against COVID-19 disease.

Several neutralizing mAbs targeting the SARS-CoV-2 Spike have entered clinical testing over the past months, yielding FDA approval of two mAb cocktails – casirivimab and imdevimab and bamlanivimab and etesevimab – for the treatment of mild to moderate COVID-19 patients⁴. In phase II/III studies, these and other mAbs that are currently awaiting regulatory approval demonstrated clear therapeutic benefit in mild to moderate COVID-19 cases, reducing the risk for hospitalization by over 80%^{1–3}. These results are in stark contrast to the findings from phase III trials (e.g. ACTIV-3, NCT04501978) that assessed the therapeutic activity of these mAbs in hospitalized COVID-19 patients. In all cases, none of the tested mAbs offered any therapeutic benefit, even when administered at exceedingly high doses or in combination with remdesivir⁵.

The antiviral activity of IgG antibodies is the outcome of Fab-mediated virus neutralization coupled with the capacity of the Fc domain to mediate effector functions through interactions with Fcγ receptors (FcγRs) expressed on effector leukocytes⁸. FcγR engagement mediates pleiotropic functions, including the clearance of viral particles⁹, the cytotoxic elimination of virus-infected cells¹⁰, as well as the induction of antiviral T-cell responses¹¹. Several reports have independently demonstrated in well-defined *in vivo* models of SARS-CoV-2 infection that the antiviral activity of neutralizing anti-SARS-CoV-2 antibodies depends on Fc-FcγR interactions^{12–15}. Additionally, mechanistic studies determined that these

protective effects are primarily mediated by CCR2⁺ monocytes, as well as cytotoxic CD8⁺ T cells that infiltrate the lung and confer antiviral activities¹². Despite these findings, no studies have explored whether optimization of neutralizing anti-SARS-CoV-2 mAbs for enhanced FcγR binding could improve their therapeutic activity, especially in the setting of severe COVID-19. Indeed, maximizing the capacity of neutralizing anti-SARS-CoV-2 mAbs to engage and activate the appropriate FcγR pathways is expected to lower the mAb dose required for the treatment of mild to moderate COVID-19, as well as improve their activity in hospitalized patients.

Currently, most mAbs in clinical use or development are expressed as human IgG1, which despite its affinity for activating FcγRs also exhibits binding to the inhibitory FcγRIIb, thereby limiting protective Fc effector activities¹¹. Additionally, due to presumptive safety concerns over the capacity of antibodies to exacerbate disease through ADE (antibody-dependent enhancement) mechanisms⁸, several clinical mAbs (etesevimab, AZD8895, and AZD1061) have been engineered to lack FcγR binding activity. However, numerous *in vivo* studies in animal models failed to provide evidence for ADE^{12–16}, and therapeutic administration of high doses of convalescent plasma or neutralizing anti-SARS-CoV-2 mAbs in COVID-19 patients has not been associated with worse disease outcomes^{1–3,5,17}. Likewise, comparable safety profiles were evident in clinical trials of neutralizing mAbs with intact or diminished Fc effector function^{3,18,19}.

¹Laboratory of Molecular Genetics and Immunology, The Rockefeller University, New York, NY, USA. ²Laboratory of Virology and Infectious Disease, The Rockefeller University, New York, NY, USA. ³Department of Epidemiology, University of North Carolina at Chapel Hill, Chapel Hill, NC, USA. ⁴Department of Microbiology and Immunology, University of North Carolina at Chapel Hill, Chapel Hill, NC, USA. ⁵These authors contributed equally: Rachel Yamin and Andrew T Jones. ⁶These authors jointly supervised this work: Jeffrey V Ravetch and Stylianos Bournazos.

✉e-mail: ravetch@rockefeller.edu; sbournazos@rockefeller.edu

Hamster FcγRs and IgG Fc domain activity

To assess the role of FcγRs in the mAb-mediated protection and develop mAbs with superior therapeutic potency, we selected well-established small animal SARS-CoV-2 infection models that recapitulate the clinical features of human COVID-19^{6,7,20}. One of these models involves the use of Syrian hamsters (*Mesocricetus auratus*), a species that sustains productive SARS-CoV-2 replication and exhibits evidence of severe disease upon challenge⁶. However, a major obstacle in the study of human IgG Fc effector activity is the substantial interspecies differences in the affinity of human IgG antibodies for FcγRs expressed by rodent species, such as hamsters²¹. We therefore cloned the four classes of hamster FcγRs and characterized their affinity for human, hamster, and mouse IgG subclasses and Fc variants (Fig. 1a, b, Extended Data Fig. 1). Comparative analysis of hamster FcγRs revealed substantial sequence homology to mouse FcγRs, with three hamster FcγRs (FcγRI, FcγRIII, FcγRIV) corresponding to activating FcγRs, whereas FcγRIIb represents the sole inhibitory FcγR.

To assess the contribution of Fc-FcγR interactions to mAb-mediated protection, we selected neutralizing mAbs in clinical use or development, including casirivimab and imdevimab (REGN cocktail²²) and S309/VIR-7831 (Vir²³) and expressed them as human IgG1 or as Fc variants with defined affinity for hamster FcγRs. In agreement with recent reports¹², we observed that when mAbs are administered prophylactically, Fc effector function has minimal contribution to the mAb antiviral activity (Fig. 1c). By contrast, in the therapy setting, wild-type, but not FcR null (GRLR) variants are able to suppress lung viremia and prevent weight loss (Fig. 1d). Since previous studies in mouse models of influenza and HIV-1 infection support a key role for FcγRIV in the mAb-mediated protection^{10,24}, we compared the *in vivo* therapeutic activity of two Fc domain variants –GAALIE and V11– that exhibit differential hamster FcγRIV binding activity, but comparable affinity for the other hamster FcγRs (Fig. 1b). Whereas the FcγRIV-enhanced variant (GAALIE) demonstrates potent antiviral activity, no therapeutic activity is evident for V11, which exhibits minimal affinity for hamster FcγRIV (Fig. 1e–g).

SARS-CoV-2 in FcγR humanized mice

Although these findings support the importance of Fc-FcγR interactions in the mAb-mediated protection against SARS-CoV-2 infection, their translational relevance is limited, given the structural complexity of the FcγR family and the divergence of these receptors between humans and other mammalian species²¹. To address this problem, we have previously developed a mouse strain in which only human FcγRs are expressed in a pattern that recapitulates as faithfully as possible the expression pattern of human tissues²⁵. Despite differences in the absolute FcγR expression levels between humans and FcγR-humanized mice (e.g. the expression of FcγRI on neutrophils and FcγRIIb on monocytes), this strain represents a suitable platform for studies on human IgG antibody function with translational relevance to humans. Human FcγR expression among the various leukocyte populations is stable and does not differ between young and old mice (Extended Data Fig. 2). Infection of old (>15 weeks old), but not young (7 weeks), FcγR humanized mice with the mouse-adapted SARS-CoV-2 strain MA10⁷ results in challenge dose-dependent weight loss and mortality (Fig. 2a, b). Recent studies determined that on day 2 post-infection, SARS-CoV-2_{MA10}-infected mice exhibit peak lung viral titers, accompanied by severely compromised pulmonary function and extensive lung histopathologic damage⁷. Histological evaluation of lungs from SARS-CoV-2_{MA10}-infected FcγR humanized mice (>15 weeks old) revealed multifocal areas of interstitial pneumonia, extensive inflammatory cell infiltration, as well as occasional necrotic and proteinaceous material and hyalinized membranes within affected alveoli (Extended Data Fig. 3). Such histopathological findings are consistent with those observed in well-established animal models of SARS-CoV-2 infection used extensively in previous studies and resemble the lung

pathology of human COVID-19^{7,12–14}. Although it is not classified as a variant of concern (VOC), the SARS-CoV-2_{MA10} strain contains several mutations near the epitopes targeted by mAbs currently in clinical use or development. As a result, several of these mAbs exhibit significantly reduced neutralizing activity against SARS-CoV-2_{MA10}, which is comparable to that observed for VOCs, like B.1.351 (Extended Data Fig. 4).

IgG Fc effector function in mAb therapy

In a model of mAb-mediated therapy, we observed that the REGN mAb cocktail (expressed as wild-type human IgG1) confers full protection of FcγR humanized mice when administered at 5 mg/kg one day after lethal challenge with SARS-CoV-2_{MA10} (Fig. 2c–f). By contrast, no therapeutic activity is evident in mice lacking FcγRs (FcγR_{null}) or when mAbs are expressed as variants (GRLR) with minimal affinity for human FcγRs, highlighting the importance of Fc effector function in the therapeutic activity of neutralizing mAbs (Fig. 2c–f). To determine the mechanisms by which human FcγRs contribute to the mAb-mediated protection, REGN cocktail mAbs were expressed as human IgG1 Fc variants¹¹ and exhibit differential affinities for the various human FcγRs (Fig. 3a). As outlined in Figure 3b, we assessed the therapeutic activity of Fc variants of the REGN mAb cocktail at a dose (1 mg/kg) which wild-type human IgG1 confers minimal protection (Fig. 3c). Consistent with a protective role for activating FcγRs, Fc variants enhanced for either FcγRIIIa (GA) or FcγRI and FcγRIII (ALIE) show a trend for improved therapeutic potency over wild-type IgG1, whereas maximal therapeutic activity was evident only for the GAALIE variant, which is enhanced for both FcγRIIIa and FcγRIII and has reduced affinity for the inhibitory FcγRIIb (Fig. 3d, e). These findings suggest that synergy between the two activating FcγRs, FcγRIIIa and FcγRIII likely accounts for the therapeutic activity of the GAALIE variant, which achieves the same degree of protection as wild-type IgG1, but at a 5-times lower dose. Additionally, the observed differences in the *in vivo* therapeutic activity among Fc variants could not be attributed to differences in their *in vitro* neutralization activity, antigen binding specificity, or *in vivo* half-life (Extended Data Fig. 5–6).

Importantly, treatment of SARS-CoV-2_{MA10}-infected mice one day post-infection with the GAALIE variant was not associated with enhanced disease not only when administered at a low dose (1 mg/kg), but also at a much higher dose (40 mg/kg) (Extended Data Fig. 7a). At this dose, which is typically used in the clinical setting, FcR null variants (GRLR) also exhibit full protective activity comparable to the GAALIE variants, suggesting that Fc-independent protection could be achieved once neutralizing mAbs are administered at sufficiently high doses, as has been documented previously for other viral pathogens²⁴. Likewise, treatment of SARS-CoV-2-infected mice two days post-infection, which coincides with the peak of lung viral replication⁷, has no disease-enhancing effects and neither GAALIE nor GRLR variants offer any therapeutic benefit, confirming recent reports that defined that the therapeutic window for neutralizing mAbs is limited to 24 hours post-infection²⁶ (Extended Data Fig. 7b).

Similar results were obtained when we assessed the *in vivo* therapeutic activity of another neutralizing anti-SARS-CoV-2 mAb cocktail (C135+C144; BMS/RU²⁷) currently in clinical development²⁷. When BMS-RU mAbs are administered to FcγR humanized mice at 1 mg/kg, only GAALIE variants, but not wild-type human IgG1 confer protective activity and prevent disease-induced weight loss (Fig. 3f, g). In contrast to neutralizing anti-SARS-CoV-2 mAbs, Fc-engineering of the non-neutralizing anti-RBD mAb, CR3022, does not result in improved therapeutic activity, as both CR3022-GAALIE and CR3022-WT failed to protect mice from lethal SARS-CoV-2 challenge (Fig. 3h).

Fc domain activity in mAb prophylaxis

Our findings in hamsters suggest that when neutralizing mAbs are administered prophylactically, Fc-FcγR interactions are not critical for

their antiviral activity (Fig. 1c). However, given the substantial interspecies differences in FcγR biology between hamsters and humans, we assessed the contribution of activating FcγR engagement to the mAb-mediated prophylaxis of SARS-CoV-2_{MA10}-challenged FcγR humanized mice (Fig. 4a). When administered at a dose where wild-type human IgG1 exhibits no protective activity (0.5 mg/kg) (Fig. 4b), GAALIE variants of the REGN mAb confer full protection against lethal SARS-CoV-2 challenge, suggesting that selective activating FcγR engagement could improve the efficacy of neutralizing mAbs both at the therapeutic as well as at the prophylactic setting (Fig. 4c).

Discussion

To maximize the translational relevance of our findings, the present study focused on neutralizing anti-SARS-CoV-2 mAbs that are currently in clinical use or development and assessed their *in vivo* protective activity in mouse strains that recapitulate the unique complexity of human FcγRs²⁵. Challenge of FcγR humanized mice with SARS-CoV-2_{MA10} results in accelerated weight loss and significant mortality, resembling the clinical manifestations of severe COVID-19. However, such rapid symptomatic disease development limits the therapeutic window for mAb treatment and does not allow to fully unravel the mechanisms of COVID-19 disease pathogenesis and the potential immunopathologies due to host immune-related responses. Despite such limitation, in the selected experimental setting, we observed that in models of mAb-mediated prophylaxis or early treatment, Fc engineering for selective binding to activating FcγRs results in approximately 5-fold reduction in the mAb dose required to achieve full therapeutic benefit; a finding consistent with our recent *in vivo* evaluation studies on Fc-optimized anti-influenza virus mAbs¹¹. Consistent with previous studies on other viral pathogens, including HIV-1²⁸, influenza²⁴, and Ebola²⁹, our findings suggest that FcγR, but not complement pathways confer mAb-mediated protection, as mAbs lack protective activity in mice deficient for all classes of FcγRs (Fig. 2c, d). Moreover, Fc variants like GAALIE, which exhibit diminished C1q binding activity (Extended Data Fig. 8), demonstrate improved therapeutic efficacy compared to wild-type IgG1.

Analysis of IgG Fc glycan characteristics in hospitalized COVID-19 patients has previously revealed an association of disease severity with elevated levels of afucosylated glycoforms^{30,31}, which exhibit increased affinity for the activating FcγRIIIb¹¹. Although these results suggest a potential pathogenic effect for FcγRIIIb pathways, severe COVID-19 patients are also characterized by delayed induction of neutralizing antibody responses yet elevated antibody levels³², suggesting that any disease-enhancing effects of afucosylated antibodies might also be related to their poor neutralizing activity³³. However, in our study, we failed to observe any pathogenic or disease-enhancing effects for anti-SARS-CoV-2 mAbs engineered for enhanced binding to activating FcγRs, irrespective of their neutralizing potency (Fig. 3). It is therefore likely that susceptibility to severe disease is not entirely driven by the FcγRIIIb binding activity of anti-SARS-CoV-2 IgGs, but rather by multiple, complex immunological determinants.

Despite the successful deployment of highly effective vaccines, neutralizing anti-SARS-CoV-2 mAbs are expected to continue to play an important role in virus containment efforts, as well as in the clinical management of COVID-19, especially in high-risk populations and immunocompromised individuals. Although regulatory approval of anti-SARS-CoV-2 mAb cocktails has been based on their remarkable clinical efficacy in mild to moderate COVID-19 patients^{1–3}, none of the currently approved mAbs take full advantage of the potential of an IgG molecule to mediate protective antiviral Fc effector functions. Our findings provide a paradigm for the development of mAb-based therapeutics with improved potency and superior therapeutic efficacy against COVID-19 through selective engagement of specific FcγR pathways.

Online content

Any methods, additional references, Nature Research reporting summaries, source data, extended data, supplementary information, acknowledgements, peer review information; details of author contributions and competing interests; and statements of data and code availability are available at <https://doi.org/10.1038/s41586-021-04017-w>.

- Chen, P. et al. SARS-CoV-2 Neutralizing Antibody LY-CoV555 in Outpatients with Covid-19. *N. Engl. J. Med.* **384**, 229–237, <https://doi.org/10.1056/NEJMoa2029849> (2021).
- Weinreich, D. M. et al. REGN-COV2, a Neutralizing Antibody Cocktail, in Outpatients with Covid-19. *N. Engl. J. Med.* **384**, 238–251, <https://doi.org/10.1056/NEJMoa2035002> (2021).
- Gottlieb, R. L. et al. Effect of Bamlanivimab as Monotherapy or in Combination With Etesevimab on Viral Load in Patients With Mild to Moderate COVID-19: A Randomized Clinical Trial. *JAMA* **325**, 632–644, <https://doi.org/10.1001/jama.2021.0202> (2021).
- Taylor, P. C. et al. Neutralizing monoclonal antibodies for treatment of COVID-19. *Nat Rev Immunol*, <https://doi.org/10.1038/s41577-021-00542-x> (2021).
- Lundgren, J. D. et al. A Neutralizing Monoclonal Antibody for Hospitalized Patients with Covid-19. *N. Engl. J. Med.* **384**, 905–914, <https://doi.org/10.1056/NEJMoa2033130> (2021).
- Sia, S. F. et al. Pathogenesis and transmission of SARS-CoV-2 in golden hamsters. *Nature*, <https://doi.org/10.1038/s41586-020-2342-5> (2020).
- Leist, S. R. et al. A Mouse-Adapted SARS-CoV-2 Induces Acute Lung Injury and Mortality in Standard Laboratory Mice. *Cell* **183**, 1070–1085.e1012, <https://doi.org/10.1016/j.cell.2020.09.050> (2020).
- Bournazos, S., Gupta, A. & Ravetch, J. V. The role of IgG Fc receptors in antibody-dependent enhancement. *Nat. Rev. Immunol.* **20**, 633–643, <https://doi.org/10.1038/s41577-020-00410-0> (2020).
- Bournazos, S. et al. Broadly Neutralizing Anti-HIV-1 Antibodies Require Fc Effector Functions for *In Vivo* Activity. *Cell* **158**, 1243–1253, <https://doi.org/10.1016/j.cell.2014.08.023> (2014).
- Lu, C. L. et al. Enhanced clearance of HIV-1-infected cells by broadly neutralizing antibodies against HIV-1 *in vivo*. *Science* **352**, 1001–1004, <https://doi.org/10.1126/science.aaf1279> (2016).
- Bournazos, S., Corti, D., Virgin, H. W. & Ravetch, J. V. Fc-optimized antibodies elicit CD8 immunity to viral respiratory infection. *Nature* **588**, 485–490, <https://doi.org/10.1038/s41586-020-2838-z> (2020).
- Winkler, E. S. et al. Human neutralizing antibodies against SARS-CoV-2 require intact Fc effector functions for optimal therapeutic protection. *Cell* **184**, 1804–1820.e1816, <https://doi.org/10.1016/j.cell.2021.02.026> (2021).
- Suryadevara, N. et al. Neutralizing and protective human monoclonal antibodies recognizing the N-terminal domain of the SARS-CoV-2 spike protein. *Cell* **184**, 2316–2331.e2315, <https://doi.org/10.1016/j.cell.2021.03.029> (2021).
- Schäfer, A. et al. Antibody potency, effector function, and combinations in protection and therapy for SARS-CoV-2 infection *in vivo*. *J. Exp. Med.* **218**, <https://doi.org/10.1084/jem.20201993> (2021).
- Ullah, I. et al. Live imaging of SARS-CoV-2 infection in mice reveals neutralizing antibodies require Fc function for optimal efficacy. *bioRxiv*, <https://doi.org/10.1101/2021.03.22.436337> (2021).
- Li, D. et al. The functions of SARS-CoV-2 neutralizing and infection-enhancing antibodies *in vitro* and in mice and nonhuman primates. *bioRxiv*, <https://doi.org/10.1101/2020.12.31.424729> (2021).
- Joyner, M. et al. Early Safety Indicators of COVID-19 Convalescent Plasma in 5,000 Patients. *medRxiv*, 2020.2005.2012.20099879, <https://doi.org/10.1101/2020.05.12.20099879> (2020).
- Dougan, M. et al. Bamlanivimab plus Etesevimab in Mild or Moderate Covid-19. *N. Engl. J. Med.*, <https://doi.org/10.1056/NEJMoa2102685> (2021).
- Wu, X. et al. Tolerability, Safety, Pharmacokinetics, and Immunogenicity of a Novel SARS-CoV-2 Neutralizing Antibody, Etesevimab, in Chinese Healthy Adults: a Randomized, Double-Blind, Placebo-Controlled, First-in-Human Phase 1 Study. *Antimicrob. Agents Chemother.* **65**, e0035021, <https://doi.org/10.1128/AAC.00350-21> (2021).
- Cleary, S. J. et al. Animal models of mechanisms of SARS-CoV-2 infection and COVID-19 pathology. *Br J Pharmacol*, <https://doi.org/10.1111/bph.15143> (2020).
- Bournazos, S. IgG Fc Receptors: Evolutionary Considerations. *Curr Top Microbiol Immunol*, https://doi.org/10.1007/82_2019_149 (2019).
- Baum, A. et al. REGN-COV2 antibodies prevent and treat SARS-CoV-2 infection in rhesus macaques and hamsters. *Science* **370**, 1110–1115, <https://doi.org/10.1126/science.abe2402> (2020).
- Pinto, D. et al. Cross-neutralization of SARS-CoV-2 by a human monoclonal SARS-CoV antibody. *Nature* **583**, 290–295, <https://doi.org/10.1038/s41586-020-2349-y> (2020).
- Dilillo, D. J., Tan, G. S., Palese, P. & Ravetch, J. V. Broadly neutralizing hemagglutinin stalk-specific antibodies require FcγR interactions for protection against influenza virus *in vivo*. *Nat. Med.* **20**, 143–151, <https://doi.org/10.1038/nm.3443> (2014).
- Smith, P., DiLillo, D. J., Bournazos, S., Li, F. & Ravetch, J. V. Mouse model recapitulating human FcγR receptor structural and functional diversity. *Proc Natl Acad Sci U S A* **109**, 6181–6186, <https://doi.org/10.1073/pnas.1203954109> (2012).
- Martinez, D. R. et al. Prevention and therapy of SARS-CoV-2 and the B.1.351 variant in mice. *Cell Rep* **36**, 109450, <https://doi.org/10.1016/j.celrep.2021.109450> (2021).
- Wang, Z. et al. mRNA vaccine-elicited antibodies to SARS-CoV-2 and circulating variants. *Nature* **592**, 616–622, <https://doi.org/10.1038/s41586-021-03324-6> (2021).

28. Hessel, A. J. et al. Fc receptor but not complement binding is important in antibody protection against HIV. *Nature* **449**, 101-104, <https://doi.org/10.1038/nature06106> (2007).
29. Bournazos, S., DiLillo, D. J., Goff, A. J., Glass, P. J. & Ravetch, J. V. Differential requirements for FcγR engagement by protective antibodies against Ebola virus. *Proc Natl Acad Sci U S A* **116**, 20054-20062, <https://doi.org/10.1073/pnas.1911842116> (2019).
30. Chakraborty, S. et al. Proinflammatory IgG Fc structures in patients with severe COVID-19. *Nat. Immunol.* **22**, 67-73, <https://doi.org/10.1038/s41590-020-00828-7> (2021).
31. Larsen, M. D. et al. Afucosylated IgG characterizes enveloped viral responses and correlates with COVID-19 severity. *Science* **371**, <https://doi.org/10.1126/science.abc8378> (2021).
32. Lucas, C. et al. Delayed production of neutralizing antibodies correlates with fatal COVID-19. *Nat Med*, <https://doi.org/10.1038/s41591-021-01355-0> (2021).
33. Atyeo, C. et al. Dissecting strategies to tune the therapeutic potential of SARS-CoV-2-specific monoclonal antibody CR3022. *JCI Insight* **6**, <https://doi.org/10.1172/jci.insight.143129> (2021).

Publisher's note Springer Nature remains neutral with regard to jurisdictional claims in published maps and institutional affiliations.

© The Author(s), under exclusive licence to Springer Nature Limited 2021

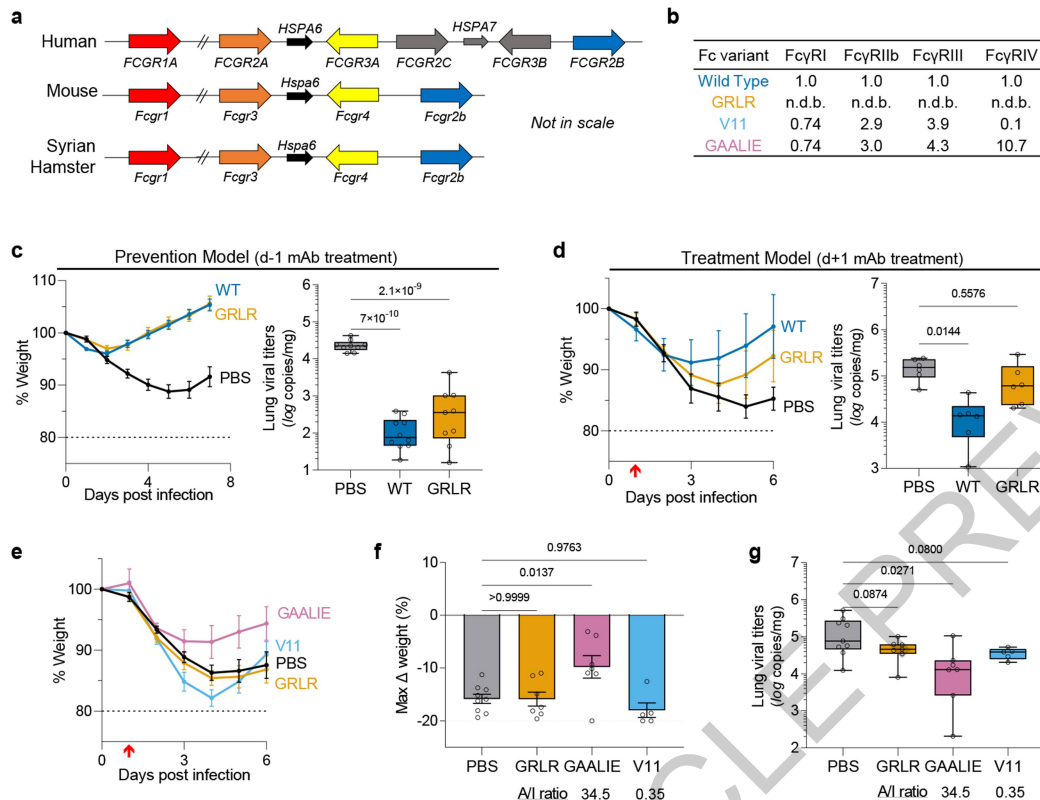


Fig. 1 | Contribution of Fc effector function to the protective activity of neutralizing anti-SARS-CoV-2 mAbs in hamster infection models.

a, Overview of the FcγR locus organization in humans, mice, and Syrian hamsters. **b**, Fc variants of human IgG1 were evaluated for their affinity for hamster FcγRs. Numbers indicate the fold-change in affinity compared to wild-type human IgG1. n.d.b., no detectable binding. **c**, **d**, Wild-type and FcR null (GRLR) variants of REGN mAb cocktail (**c**) or S309 mAb (**d**) were administered i.v. (5 mg/kg) to Syrian hamsters one day before (prevention model, **c**) or after (therapy model, **d**) i.n. challenge with SARS-CoV-2 (NYC isolate, 10^5 pfu) ($n = 9$ hamsters per group for PBS and GRLR-treated, $n = 10$ for wild-type from two independent experiments for **c** and $n = 6$ hamsters per group from two independent experiments for **d**). Hamsters were monitored for weight loss (left; mean \pm s.e.m.) and lung viral titers (right, analyzed on day 7 (**c**

or 6 (**d**) post-infection) were compared between treatment groups by one-way ANOVA (Bonferroni post hoc analysis adjusted for multiple comparisons). P values are indicated. **e–g**, SARS-CoV-2-infected hamsters (10^5 pfu, NYC isolate) were treated on day 1 post-infection with Fc variants of the REGN mAb cocktail (5 mg/kg, i.v.) exhibiting differential hamster FcγR binding affinity and A/I ratio (calculated based on FcγRIV/FcγRIIb affinity). Weight loss (**e**, plotted over time (mean \pm s.e.m.) or **f**, as max change) and lung viral titers (**g**, assessed on day 6 post-infection) were compared by one-way ANOVA (Bonferroni post hoc analysis adjusted for multiple comparisons). P values are indicated. $n = 9$ hamsters per group for PBS-treated, $n = 7$ for GRLR and GAALIE, and $n = 5$ for V11 from two independent experiments. Red arrow indicates time point of mAb treatment post-infection. Boxes and whiskers represent the median, quartiles, and range (minimum to maximum).

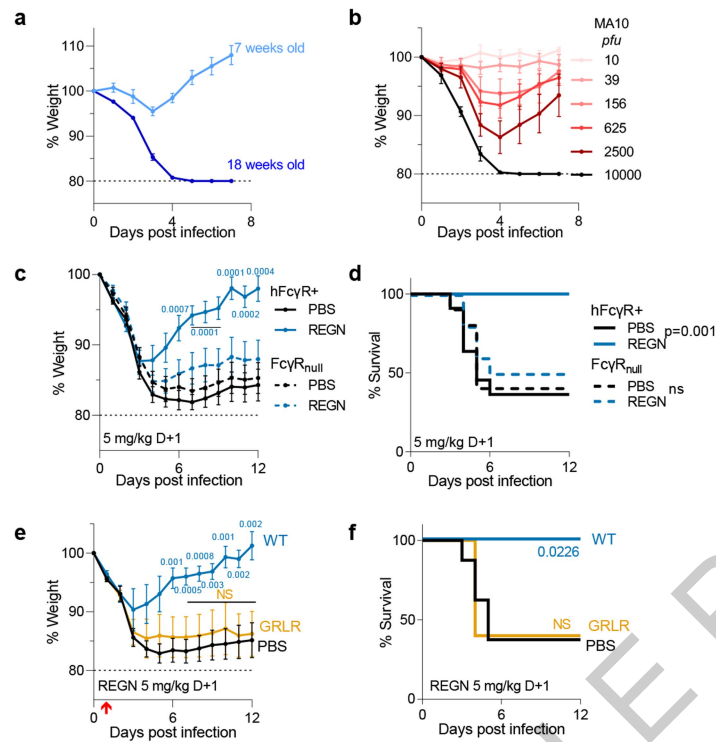


Fig. 2 | Fc-Fc γ R interactions are required for the therapeutic activity of neutralizing anti-SARS-CoV-2 mAbs in mouse infection models. a, b, Fc γ R humanized mice were infected with mouse-adapted SARS-CoV-2 (MA10 strain, 10^4 pfu, i.n.) and weight loss (mean \pm s.e.m.) was compared in (a) young (7 weeks old; n = 5) and older (18 weeks old; n = 4) mice, as well as in (b) mice (16–19 weeks old) challenged with the indicated inoculum dose. n = 5 mice per group; n = 4 for 10^4 and 10 pfu dose groups from two independent experiments. c, d, The therapeutic activity of REGN mAb cocktail (expressed as human IgG1 and administered at 5 mg/kg one day post-infection) was evaluated in Fc γ R humanized and Fc γ R deficient (Fc γ R $_{null}$) mouse strains challenged with SARS-CoV-2 (MA10 strain, 10^4 pfu i.n.). n = total of 10 mice per group for Fc γ R $_{null}$

and n = total of 11 (PBS) and n = 12 (REGN) mice per group for Fc γ R humanized mice from two independent experiments. e, f, SARS-CoV-2-infected Fc γ R humanized mice (MA10 strain, 10^4 pfu i.n.) were treated with wild-type human IgG1 or GRLR variants of REGN mAb cocktail one day post-infection. n = total of 8 (PBS), 5 (WT), and 6 (GRLR) mice per group from two independent experiments. Weight loss (c, e; mean \pm s.e.m.) and survival curves (d, f) were compared to the corresponding PBS-treated group by two-way ANOVA (Bonferroni post hoc analysis adjusted for multiple comparisons) and log-rank (Mantel–Cox) test, respectively. P values are indicated. NS, not significant. Red arrow indicates time point of mAb treatment post-infection.

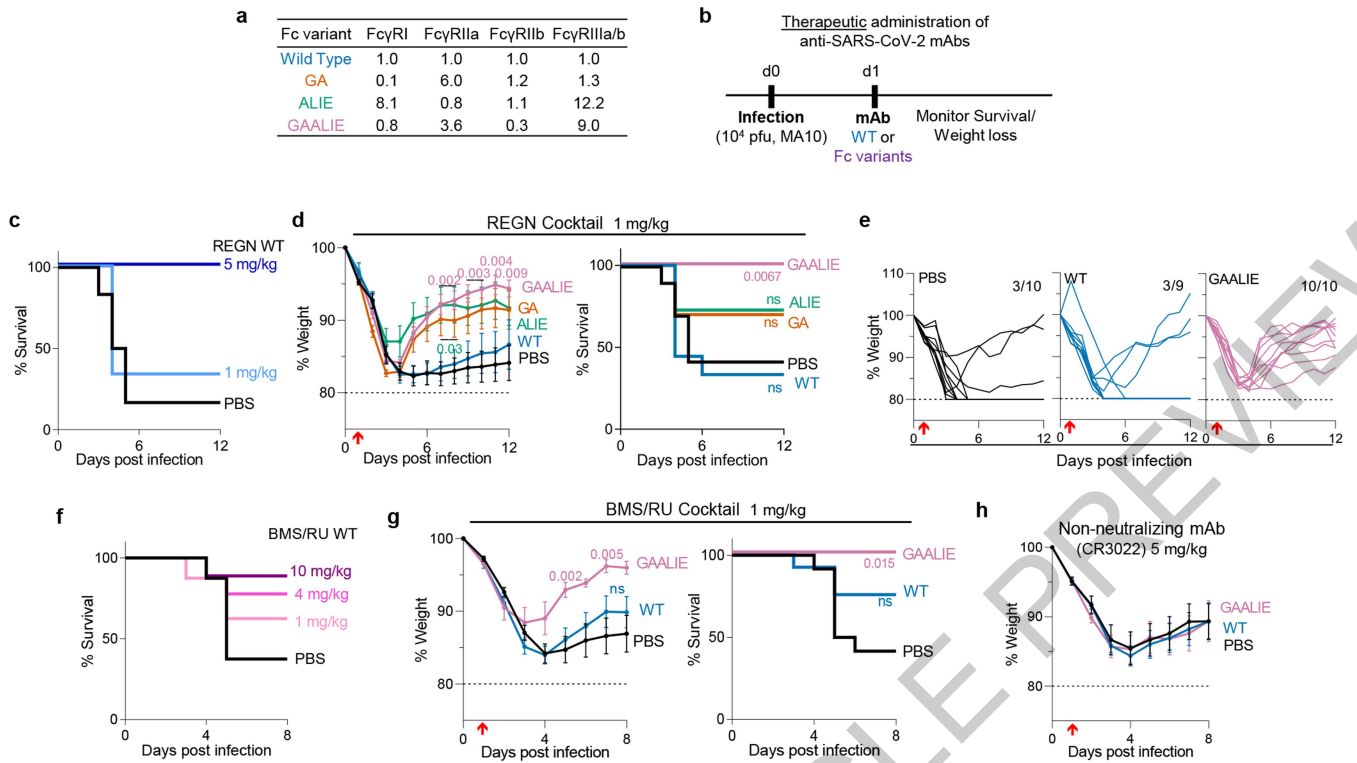


Fig. 3 | Selective engagement of activating FcγRs improves the therapeutic activity of anti-SARS-CoV-2 mAbs. **a**, Human IgG1 Fc variants with differential affinity for specific classes of human FcγRs were generated for anti-SARS-CoV-2 mAbs. Numbers indicate the fold-change in affinity compared to wild-type human IgG1. **b–g**, Following the experimental strategy in panel **b**, SARS-CoV-2-infected FcγR humanized mice were treated (i.v.) at the indicated dose with REGN (**c–e**) or BMS/RU (**f, g**) mAb cocktail, or the non-neutralizing mAb CR3022 (**h**), expressed as wild-type human IgG1 or as Fc variants with differential affinity for human FcγRs. Weight loss (mean ± s.e.m.) (**h** and **d, g**, left panels; **e**, curves from individual mice) and survival curves (**c, f** and **d, g**, right panels) of antibody-treated mice were compared with the corresponding PBS-treated

group by two-way ANOVA (Bonferroni post hoc analysis adjusted for multiple comparisons) and log-rank (Mantel–Cox) test, respectively. P values are indicated. NS, not significant. **c**, n = 6 mice per group from two independent experiments; **d, e**, n = total of 10 mice per group (for PBS, GAALIE, GA groups), n = 9 for WT, and n = 11 for ALIE from four independent experiments; **f**, n = total of 8 (PBS and 1 mg/kg) or 9 (10 mg/kg and 4 mg/kg groups) mice per group from two independent experiments; **g**, n = total of 7 (GAALIE) or 12 (PBS, WT) mice per group from three independent experiments. **h**, n = total of 8 (GAALIE) or 10 (PBS, WT) mice per group from two independent experiments. Red arrow indicates time point of mAb treatment post-infection.

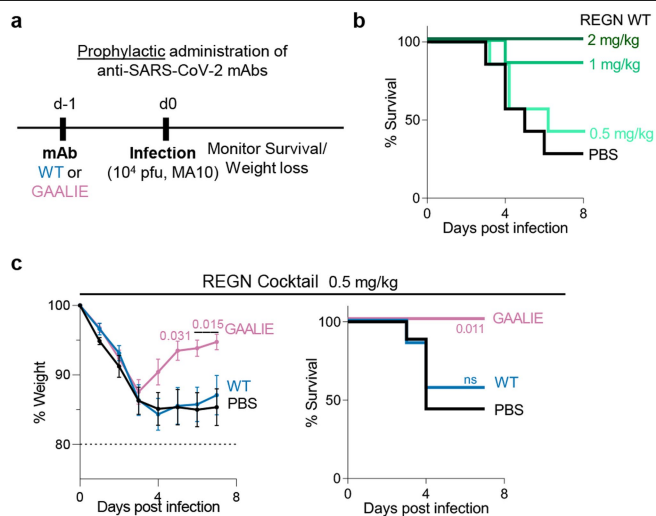


Fig. 4 | Prophylactic activity of anti-SARS-CoV-2 mAbs is enhanced by selective engagement of activating FcγRs. In a model of mAb-mediated prophylaxis of SARS-CoV-2 infection (a), the activity of wild-type and GAALIE variants of the REGN mAb cocktail was assessed. FcγR humanized mice were treated (i.v.) at the indicated dose with REGN mAb cocktail expressed as wild-type human IgG1 or as GAALIE variant one day prior to challenge with SARS-CoV-2 (MA10, 10⁴ pfu i.n.). Weight loss (mean ± s.e.m.) (c, left panel) and survival curves (b and c, right panel) of antibody-treated mice were compared with the PBS-treated group by two-way ANOVA (Bonferroni post hoc analysis adjusted for multiple comparisons) and log-rank (Mantel–Cox) test, respectively. P values are indicated. NS, not significant. **b**, n= total of 7 mice per group (n = 6 mice/group for 2 mg/kg) from two independent experiments; **c**, n= total of 7 (WT) or 9 (PBS, GAALIE) mice per group from three independent experiments.

Methods

Viruses, Cell Lines, and Animals

A P1 stock of the SARS-CoV-2 MA10 strain⁷ was amplified in VeroE6 cells obtained from the ATCC that were engineered to stably express TMPRSS2 (VeroE6_{TMPPRSS2}). To generate a P2 working stock, VeroE6_{TMPPRSS2} cells were infected at a multiplicity of infection (MOI) of 0.1 plaque forming units (pfu)/cell and incubated at 37 °C for 4 days. The virus-containing supernatant was subsequently harvested, clarified by centrifugation (3,000 g; 10 min), and filtered using a disposable vacuum filter system with a 0.22 μm membrane. Virus stock titers were measured by standard plaque assay on Huh-7.5 cells that stably express ACE2 and TMPRSS2 (Huh-7.5_{ACE2/TMPRSS2}). Briefly, 500 μl of serial 10-fold virus dilutions in Opti-MEM were used to infect 4 × 10⁵ cells seeded the day prior into wells of a 6-well plate. After 90 min adsorption, the virus inoculum was removed, and cells were overlaid with DMEM containing 10% FBS with 1.2% microcrystalline cellulose (Avicel). Cells were incubated for four days at 33 °C, followed by fixation with 7% formaldehyde and crystal violet staining for plaque enumeration. To confirm virus identity and evaluate for unwanted mutations that were acquired during the amplification process, RNA from virus stocks was purified using TRIzol Reagent (ThermoFisher). Briefly, 200 μl of each virus stock was added to 800 μl TRIzol Reagent, followed by 200 μl chloroform, which was then centrifuged at 12,000 g for 5 min. The upper aqueous phase was moved to a new tube, mixed with an equal volume of isopropanol, and then added to an RNeasy Mini Kit column (Qiagen) to be further purified following the manufacturer's instructions. Viral stocks were subsequently confirmed via next generation sequencing using libraries for Illumina MiSeq.

The SARS-CoV-2 NYC isolate was obtained from a patient's saliva generously provided by Agnès Viale (Memorial Sloan Kettering Cancer Center) and amplified in Caco-2 cells. This P1 virus was used to generate a P2 working stock by infecting Caco-2 cells at a MOI of 0.05 pfu/cell. Cells were incubated at 37 °C for 6 days before harvesting virus-containing supernatant as described above. Similarly, virus stock titers were determined by plaque assay performed on Huh-7.5_{ACE2/TMPRSS2} cells. All SARS-CoV-2 experiments were carried out in biosafety level 3 (BSL-3) containment in compliance with institutional and federal guidelines.

VeroE6 cells (ATCC, CRL-1586), Caco-2 cells (ATCC, HTB-37), and Huh-7.5 hepatoma cells (described in³⁴) were cultured in Dulbecco's Modified Eagle Medium (DMEM) supplemented with 1% nonessential amino acids (NEAA) and 10% fetal bovine serum (FBS). 293T cells (ATCC, CRL-3216) and HT1080_{ACE2} (kindly provided by Dr. Paul Bieniasz, Rockefeller University) were maintained in DMEM supplemented with 10% FBS, 50 U/ml penicillin and 50 μg/ml streptomycin (ThermoFisher). All cell lines were maintained at 37 °C at 5% CO₂. Expi293F cells (ThermoFisher) were maintained at 37 °C, 8% CO₂ in Expi293 expression medium (ThermoFisher) supplemented with 10 U/ml penicillin and 10 μg/ml streptomycin. Cell lines were not authenticated after purchase. All cell lines have been tested negative for mycoplasma contamination.

In vivo experiments were approved by the Rockefeller University Institutional Animal Care and Use Committee in compliance with federal laws and institutional guidelines. Hamsters and mice were maintained at the Comparative Bioscience Center at the Rockefeller University at a controlled ambient temperature (20–25 °C) and humidity (30–70%) environment with 12-h dark/light cycle. Golden Syrian hamsters were purchased from Charles River laboratories (strain code 049) and maintained in compliance with USDA regulations. FcγR knockout (mFcγRα^{-/-}; FcγRI^{-/-}) and FcγR humanized mice (mFcγRα^{-/-}, FcγRI^{-/-}, hFcγRI⁺, hFcγRIIa_{R131}⁺, hFcγRIIb⁺, hFcγRIIIa_{F158}⁺, and hFcγRIIIb⁺) were generated in the C57BL/6 background and characterized in previous studies^{11,25}.

Cloning, Expression, and Purification of Recombinant Proteins

Human IgG1 Fc domain variants were generated by site-directed mutagenesis using specific primers as previously described⁹ and

recombinant IgG antibodies were expressed and purified using previously described protocols¹¹. Purity was assessed by SDS-PAGE followed by SafeStain blue staining (ThermoFisher), as well as by size exclusion chromatography (SEC) using a Superdex 200 Increase 10/300GL column (GE Healthcare) on an Äkta Pure 25 HPLC system (data analyzed using Unicorn v.6.3 software). All antibody preparations were more than 94% pure and endotoxin levels were less than 0.05 EU/mg, as measured by the limulus amoebocyte lysate assay.

The two plasmid-based HIV/NanoLuc-SARS-CoV-2 pseudovirus system was kindly provided by Dr. Paul Bieniasz (described in³⁵). The S gene was modified by site-directed mutagenesis to introduce the amino acid changes present in the MA10 or the B.1.351 strains⁷. SARS-CoV-2_{WT}, SARS-CoV-2_{MA10} and SARS-CoV-2_{B.1.351} pseudovirus particles were generated by transfection of the two plasmid-based system to 293T cells using X-tremeGENE HP DNA transfection reagent (Sigma).

Golden Syrian hamster FcγR cDNA sequences were identified based on the current *Mesocricetus auratus* genome assembly (MesAur1.0) and recent transcriptomic data³⁶. To validate sequences, hamster FcγR sequences were amplified and sequenced (Genewiz) from Syrian hamster spleen cDNA (Zyagen) using the following primers: hamster FcγRI (5'-GGC GGA CAA GTG GTA AAT GTC AC-3', 5'-CGG ACA CAT CAT TGC TTC AGA CTT ACT AAG-3'), hamster FcγRII (5'-CTG CTG GGA CAC ATG ATC TCC-3', 5'-TTA AAT GTG GTT CTG GTA ATC ATG CTC TG-3'), hamster FcγRIII (5'-GAG TCT GGA GAC ACA GAT GTT TCA G-3', 5'-CGA CGT CAT TTG TCC CGA GG-3'), hamster FcγRIV (5'-AAT GGG TGA GGG TGC TTG AG-3', 5'-GAG GGA ATG TTG GGG ACA GG-3'). To identify the ectodomain, transmembrane, and cytoplasmic domains, Syrian hamster FcγR protein sequences were then aligned against annotated mouse FcγR protein sequences (Uniprot). Soluble Syrian hamster FcγR ectodomains were generated by transient transfection as described above for mAbs. Syrian hamster FcγR expression plasmids were generated encoding a secretion signal peptide, the predicted Syrian hamster FcγR ectodomain, and a C-terminal Strep or His tag. Following transfection of Expi293 cells, recombinant FcγRs were purified from cell-free supernatants by affinity purification using Strep-Tactin Superflow Plus resin (Qiagen) or Ni-NTA Agarose (Qiagen), per manufacturer's instructions. Purified proteins were dialyzed into PBS and assessed for purity by SDS-PAGE gel electrophoresis followed by SafeStain blue staining. Monomeric FcγR ectodomains were fractionated from aggregates by size exclusion chromatography on an Äkta Pure system using a Superdex 200 Increase 10/300 GL column (GE Healthcare).

Surface Plasmon Resonance

All experiments were performed with a Biacore T200 SPR system (GE Healthcare) at 25 °C in HBS-EP⁺ buffer (10 mM HEPES, pH 7.4, 150 mM NaCl, 3.4 mM EDTA, 0.005% (v/v) surfactant P20). IgG antibodies were immobilized on Series S Protein G sensor chip (GE Healthcare) at a density of 2,000 response units (RU). Serial dilutions of recombinant soluble hamster FcγR ectodomains were injected to the flow cells at 20 μl/min, with the concentration ranging from 1000 to 15.625 nM (1:2 successive dilutions). Association time was 60 s followed by a 900-s dissociation step. At the end of each cycle, sensor surface was regenerated with a glycine HCl buffer (10 mM, pH 2.0; 50 μl/min, 30 s). Background binding to blank immobilized flow cells was subtracted, and affinity constants were calculated using BIAcore T200 evaluation software v.2.0 (GE Healthcare) using the 1:1 Langmuir binding model.

Neutralization Assay

Neutralization activity of IgG1 Fc domain variants was measured as previously described³⁵. Briefly, HT1080_{ACE2} cells were seeded in 96 U-well black plates 24 h prior to infection with SARS-CoV-2_{WT}, SARS-CoV-2_{MA10} or SARS-CoV-2_{B.1.351} pseudoviruses. Pseudovirus particles were pre-incubated with mAbs (four-fold serially diluted starting at 10 μg/ml) for 1 h at 37 °C and then added to a monolayer of HT1080_{ACE2} cells. Following a 48-h incubation at 37 °C, cells were carefully washed with

Article

PBS and lysed with Luciferase Cell Culture Lysis reagent (Promega) for 15 min. Nano luciferase activity was detected by adding Nano-Glo Luciferase Assay System (Promega) and measured by SpectraMax Plus spectrophotometer (Molecular Devices), using 0.5 s integration time. Data were collected and analyzed using SoftMax Pro v.7.0.2 software (Molecular Devices). Relative luciferase units were normalized to those derived from cells infected with the relevant SARS-CoV-2 pseudoviruses in the absence of mAbs.

Anti-SARS-CoV-2 RBD ELISA

Recombinant SARS-CoV-2 RBD was immobilized (1 µg/ml) into high-binding 96-well microtitre plates (Nunc) and after overnight incubation at 4 °C, plates were blocked with PBS plus 2% (w/v) BSA for 2 h. After blocking, plates were incubated for 1 h with serially diluted IgG antibodies or serum samples (1:3 consecutive dilutions in PBS starting at 100 ng/ml), followed by HRP-conjugated goat anti-human IgG (1 h; 1:5,000; Jackson ImmunoResearch). Plates were developed using the TMB two-component peroxidase substrate kit (KPL) and reactions were stopped with the addition of 1 M phosphoric acid. Absorbance at 450 nm was immediately recorded using a SpectraMax Plus spectrophotometer (Molecular Devices) and background absorbance from negative control samples was subtracted. Data were collected and analyzed using SoftMax Pro v.7.0.2 software (Molecular Devices).

C1q Binding Assay

Human and mouse C1q binding to IgG1Fc variants was assessed following previously described protocols³⁷. Briefly, antibodies were serially diluted (100–0.046 µg/ml) in PBS and coated overnight (4 °C) onto high-binding 96-well microtiter plates. After washing with PBS+0.05% Tween-20, plates were blocked with 2% BSA. Normal mouse or human serum (3%) was added and incubated for 60 min with gentle shaking. For the detection of C1q binding, monoclonal mouse anti-C1q antibody (JL-1, Abcam) was added at 0.5 µg/ml, HRP-conjugated goat anti-mouse IgG was used at a dilution of 1:5000, and plates were developed and analyzed as described above.

Quantification of Serum IgG Levels

Blood was collected into microvette serum gel tubes (Sarstedt) and serum was fractionated by centrifugation (10,000 g, 5 min). IgG levels were determined by ELISA following previously described protocols¹¹.

In vivo SARS-CoV-2 Infection Models

All animal infection experiments were performed at the Comparative Bioscience Center of the Rockefeller University in animal biosafety level 3 (ABSL-3) containment in compliance with institutional and federal guidelines. Hamsters (males; 6–8 weeks old) were anaesthetized with isoflurane (3%) in a VetFlo high-flow vaporizer followed by an intraperitoneal injection of a ketamine (150 mg/kg) and xylazine (10 mg/kg) mixture. Hamsters were challenged intranasally with 10⁵ pfu SARS-CoV-2 (NYC isolate, 100 µl viral inoculum). Mice (males or females; 6–7 or 16–22 weeks old) were anaesthetized with a ketamine (75 mg/kg) and xylazine (15 mg/kg) mixture (administered intraperitoneally) prior to challenge with SARS-CoV-2 (MA10 strain, 10⁴ pfu in 30 µl, intranasally).

No statistical method was used to predetermine sample size. Based on preliminary studies that determined experimental variation in survival following infection and mAb treatment, we have performed power calculations and determined that at least n = 6 animals/group is sufficient to detect differences among experimental groups (powered at 80% for 5% significance level; survival assessed by log-rank (Mantel-Cox) test).

After infection, animals were monitored daily and humanely euthanized by CO₂ asphyxiation at endpoints authorized by the Rockefeller University Institutional Animal Care and Use Committee, including any of the following: marked lethargy or inactivity, severe respiratory distress or labored breathing, inability to ambulate, and weight loss

of greater than 20% of baseline. Animals were randomized based on age, gender, and weight. Before treatment, we ensured that the mean weight, gender, and age were comparable among the various treatment groups. The treatment groups were not blinded to the personnel involved in monitoring animal survival and weight upon challenge. For antibody-mediated prophylaxis, antibodies were administered intravenously one day before virus challenge, whereas for antibody-mediated therapy, antibodies were administered one day after infection. Antibody dose was calculated as mg/kg.

Histological Analysis

Lungs from euthanized mice were instilled with 10% neutral buffered formalin and fixed overnight by submersion in 10% formalin. Fixed tissues were embedded in paraffin, sectioned at 4 µm thickness, and stained with hematoxylin and eosin. Sections of lung were microscopically evaluated by a board-certified veterinary anatomic pathologist and representative images were captured with an Olympus BX45 light microscope using an SC30 camera with the cellSens Dimension software.

Determination of Lung Viral Titers

Hamsters were euthanized at the indicated timepoints following infection and lung weights were recorded. Lungs were lysed in Trizol (ThermoFisher) and dissociated in gentle MACS M tubes using the gentleMACS Octo Dissociator (Miltenyi Biotec). Samples were transferred into Phasemaker tubes (ThermoFisher) and chloroform was added (200 µl chloroform/1 ml Trizol). After vigorous shake, tubes were rested for 5 min and then centrifuged for 15 min at 12,000 g at 4 °C. The aqueous phase containing the RNA was transferred into a new tube and RNA extraction was performed by using RNeasy mini kit (Qiagen). SARS-CoV-2 lung titers were determined by qRT-PCR assay using TaqMan Fast Virus 1-Step Master Mix and specifically designed primers and a TaqMan probe that bind a conserved region in the nucleocapsid gene of SARS-CoV-2 (2019-nCoV_N1-F: 5'-GAC CCC AAA ATC AGC GAA AT-3'; 2019-nCoV_N1-R: 5'-TCT GGT CAT TGC TGG AAT CTG-3'; 2019-nCoV_N1-P: 5'-FAM-ACC CCG CAT TAC GTT TGG ACC-BHQ1-BHQ1-3'). qPCR was performed using an Applied Biosystems QuantStudio 6 Flex cyclor using the following parameters: 50 °C for 5 min, 95 °C for 20 s followed by 40 cycles of 95 °C for 3 s, and 30 s at 60 °C. Signal from unknown samples was compared to a known standard curve (obtained through BEI Resources, NIAID, NR-52358) and viral titers were expressed as RNA copies/mg tissue.

Flow Cytometry

After lysis of red blood cells (RBC lysis buffer; Biolegend), cells were resuspended in PBS containing 0.5% (w/v) BSA and 5 mM EDTA and labelled with the following fluorescently labelled antibodies (all used at 1:200 dilution unless otherwise stated): anti-human FcγRIIIa (clone IV.3)-FITC, anti-human FcγRIIb (clone 2B6)-Dylight650 (used at 5 µg/ml), anti-B220-AlexaFluor700, anti-Gr1-BrilliantViolet421, anti-CD8β-BrilliantViolet510, anti-human FcγRI (clone 10.1)-BrilliantViolet605, anti-CD3-BrilliantViolet650 (used at 1:100 dilution), anti-CD11b-BrilliantViolet711, anti-CD4-BrilliantViolet785, anti-human FcγRIIIa/b (clone 3G8)-PE, and anti-NK1.1-PE/Cy7. Relevant isotype control antibodies were used and included: mouse IgG1 isotype control-Dylight650 (used at 5 µg/ml), mouse IgG2b kappa isotype control-FITC, mouse IgG1 kappa isotype control-PE, mouse IgG1 kappa isotype control-BrilliantViolet605. Samples that were stained with isotype control antibodies were also blocked with unlabeled anti-FcγR antibodies as follow: anti-human FcγRI (clone 10.1), anti-human FcγRIIIa (clone IV.3), anti-human FcγRIIb (clone 2B6), and anti-human FcγRIIIa/b (clone 3G8) (used at 10 µg/ml and incubated for 5 min prior to staining with fluorescently labelled antibodies). Samples were analyzed on an Attune NxT flow cytometer (ThermoFisher) using Attune NxT software v3.1.2 and data were analyzed using FlowJo (v10.7) software.

Statistical Analysis

Raw data for all main and extended data figures are included in the manuscript as source files. Results from multiple experiments are presented as mean \pm s.e.m. One- or two-way ANOVA was used to test for differences in the mean values of quantitative variables, and where statistically significant effects were found, post hoc analysis using Bonferroni (adjusted for multiple comparisons) test was performed. Statistical differences between survival rates were analyzed by comparing Kaplan–Meier curves using the log-rank (Mantel–Cox) test. Data were collected and analyzed with Microsoft Excel and GraphPad Prism v.9.1 software (GraphPad) and $p < 0.05$ were considered to be statistically significant.

Reporting summary

Further information on research design is available in the Nature Research Reporting Summary linked to this paper.

Data availability

Raw data for all main and extended data figures are included in the manuscript as source files. Source data are provided with this paper.

34. Blight, K. J., McKeating, J. A. & Rice, C. M. Highly permissive cell lines for subgenomic and genomic hepatitis C virus RNA replication. *J Virol* **76**, 13001-13014, <https://doi.org/10.1128/jvi.76.24.13001-13014.2002> (2002).
35. Schmidt, F. et al. Measuring SARS-CoV-2 neutralizing antibody activity using pseudotyped and chimeric viruses. *J Exp Med* **217**, <https://doi.org/10.1084/jem.20201181> (2020).
36. McCann, K. E., Sinkiewicz, D. M., Norvelle, A. & Huhman, K. L. De novo assembly, annotation, and characterization of the whole brain transcriptome of male and female Syrian hamsters. *Sci. Rep.* **7**, 40472, <https://doi.org/10.1038/srep40472> (2017).
37. Pietzsch, J. et al. A mouse model for HIV-1 entry. *Proc Natl Acad Sci U S A* **109**, 15859-15864, <https://doi.org/10.1073/pnas.1213409109> (2012).

Acknowledgements We would like to thank Patrick Smith, Emily Lam, Ruben Peraza, Luke Smith, Adriana Martin Mozqueda, and Tiffany Martinez (Rockefeller University) for technical assistance and for maintaining and genotyping the mouse colonies used in this study and all the members of the Laboratory of the Molecular Genetics and Immunology (Rockefeller University) for discussions. We also thank Sara Borghi (Rockefeller University) for providing the recombinant SARS-CoV-2 RBD, Paul Bieniasz (Rockefeller University) for providing the HT1080_{ACE2} cell line and plasmids for generating pseudoviruses, Agnès Viale (Memorial Sloan Kettering Cancer Center) for providing the SARS-CoV-2 NYC clinical isolate, Alison Ashbrook and Gaitree McNab (Rockefeller University) for advice on handling BSL-3 agents and processing of tissues from infected animals, David Martinez (University of North Carolina at Chapel Hill) for technical assistance, and Sebastian Carrasco (Memorial Sloan Kettering Cancer Center/Weill Cornell Medicine) and staff from the Laboratory Comparative Pathology for histopathology support (with funding from NIH Core Grant P30CA008748). Research reported in this publication was supported by the National Institute of Allergy and Infectious Diseases (R01AI137276, R01AI157155, U19AI111825, and R01AI145870) and the Bill and Melinda Gates Foundation (INV-023152). This work was in part made possible with funding from the G. Harold and Leila Y. Mathers Charitable Foundation, the Bawd Foundation, and Fast Grants (www.fastgrants.org), a part of Emergent Ventures at the Mercatus Center, George Mason University. We acknowledge support from the Rockefeller University and Vir Biotechnology Inc. The content is solely the responsibility of the authors and does not necessarily represent the official views of the NIH.

Author contributions R.Y. designed and performed experiments, generated reagents, and analyzed the data; A.T.J. cloned and characterized hamster FcγRs, performed binding studies, and analyzed data; H.-H.H. and A.S. generated and characterized virus stocks; K.S.K. generated reagents, performed *in vitro* experiments, and analyzed the data; R.L.F. designed and performed *in vivo* experiments and generated reagents; T.P.S., R.S.B., and C.M.R. provided intellectual input; J.V.R. designed and directed the study; S.B. designed experiments, analyzed data, directed the study, and wrote the manuscript with input and edits from all co-authors.

Competing interests S.B. and J.V.R. are inventors on a patent (WO2019125846A1) describing the GAALIE variant and its use in therapeutic mAbs. C.M.R. and J.V.R. are SAB members of Vir Biotechnology with equity interests.

Additional information

Supplementary information The online version contains supplementary material available at <https://doi.org/10.1038/s41586-021-04017-w>.

Correspondence and requests for materials should be addressed to Jeffrey V. Ravetch or Stylianos Bourazos.

Peer review information Nature thanks Patrick Wilson and the other, anonymous reviewers for their contribution to the peer review of this work. Peer reviewer reports are available.

Reprints and permissions information is available at <http://www.nature.com/reprints>.

a

Syrian hamster FcγRI

MWLLTTLLLLVVGVGQVVNVTKAVVTLQPPWVSIFLKNVTLWCEGLHPP
GDPTTRWF INSTALQISTPSYS ITEATLKDSGEYRCOTGLSMSPDPVOLE
IHRDWLLQASDRVLTEGCPLTRCHGWQSKMVNVVFYRDGKYFHSSOD
SEVTLLOTNLTHSGVYHCAGIGRHYHRYTSAGMSVTVKELFATPVLTASL
SSPFFEGSPVTLCSVYKLPPQSPGLQLYFSFYVGSETLEDRKTSAEYHILP
SAKREDSGLYWCEAATDGSYRKRSPELELRTPGSSGPVWFHLFYLS
MGIFIVDTVLCAKIRKKLQRKNYNLEVLVSDQKKETSS

Syrian hamster FcγRIIb

MLLWTAVLNLAAGTHDLPKAMKLEPPWIQVLKEDRVTLKCEGTHSPGND
STOWLHNGNSLWSOVQPSYTFKASDNDSGEYQCRMGOTSLSDPVOLGVIS
DNLLLOTPOLVFEEGETIVLRCHSWRNKFMSKVTFYHNGSIRYNHFISN
VSIAKANHSHSGDYHCTARLGOAHSRPVTITVOEPRSSGSLPILTIVA
AVTGIAVAAVILVSLIYLKRQAPALPGNPDHREKGDTLPKEQEYSV
PSGDSVFVSRPFCQEPASNSYNSPOLEAAKTEVENTITYSLLKHPE
APDEAEHDYQNHI

Syrian hamster FcγRIII

MFQNVHSGSQWLLQPLTILLLFALADRQTADLEKAVVKLEPPWIQVLKED
RVTLKCEGTHSPGNDWLHNGNSLWSOVQPSYTFKASDNDSGEYQCRM
GOTSLSDPVOLGVISDNLLOTPOLVFEEGETIVLRCHSWRNKFMSKVT
YHNGSIRYNHFISNISTAKANHSHSGDYHCTARLGOAHSRPVTITVO
GESTTFFTSLWHAAFLMCLLFAVDTGLYFYVQRNLQAPEKWRKTL
SVRKQAPRDK

Syrian hamster FcγRIV

MWQLLPTALLLIVSSGIRAGLRKAVVTLPPEWRVLEEDSVTLRCQTY
APGDNSTKWFHNGSLTSODTNVIGSAKVDSGEYKOTALSTASDPVN
LEVHIGWLLOTORPVFOEGDPTRLKCHSWRNKTVYKVTLQNGKGKY
FHKNSELVIPNATONHSGSYFCRGLIGONNKSSETLRIVGVLPPDLTP
SNNFPWHQITCLLIGLLFTIDVLFSVQRLRRSTADYEEPDLHSK
EPEDKTISEEKQSFRSRNSTPSGSRPEK

b

Human IgG1 Fc Variant	FcγRI		FcγRIIb		FcγRIII		FcγRIV	
	KD (M)	Fold	KD (M)	Fold	KD (M)	Fold	KD (M)	Fold
Wild Type	7.37×10^{-7}	1.00	$>1.0 \times 10^{-6}$	1.00	$>1.0 \times 10^{-6}$	1.00	1.02×10^{-7}	1.0
V11	$>1.0 \times 10^{-6}$	<0.74	3.45×10^{-7}	>2.9	2.60×10^{-7}	>3.9	$>1.0 \times 10^{-6}$	<0.1
GAALIE	$>1.0 \times 10^{-6}$	<0.74	3.28×10^{-7}	>3.0	2.33×10^{-7}	>4.3	9.52×10^{-9}	10.7
GRLR	n.d.b.		n.d.b.		n.d.b.		n.d.b.	

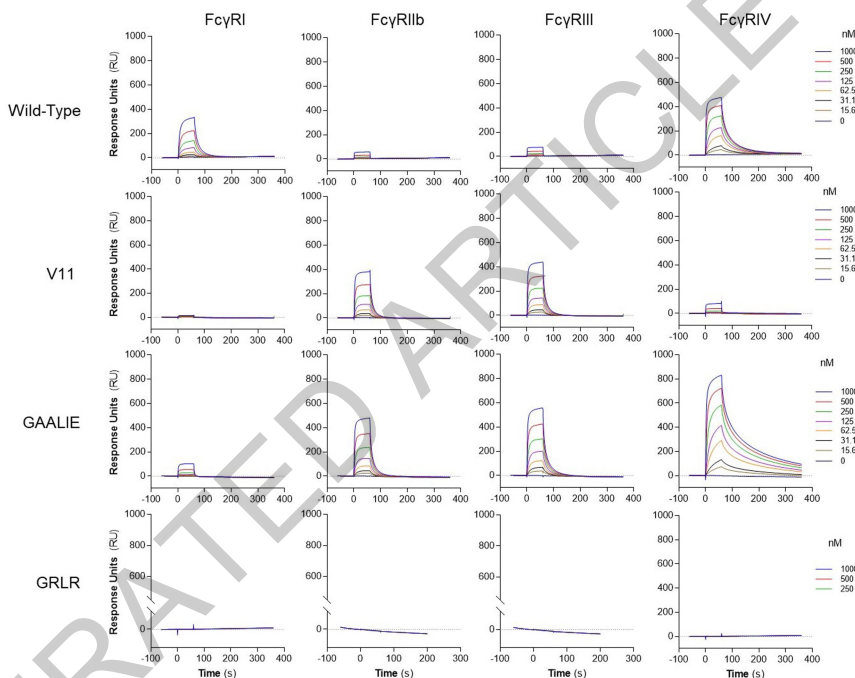
c

Mouse IgG	FcγRI		FcγRIIb		FcγRIII		FcγRIV	
	KD (M)	Fold	KD (M)	Fold	KD (M)	Fold	KD (M)	Fold
IgG1	$>1.0 \times 10^{-6}$	1.0	1.43×10^{-7}	1.0	7.81×10^{-8}	1.0	$>1.0 \times 10^{-6}$	1.0
IgG2a	3.38×10^{-7}	>3.0	1.14×10^{-6}	0.12	5.72×10^{-7}	0.13	1.47×10^{-8}	>68
IgG1-D265A	n.d.b.		n.d.b.		n.d.b.		n.d.b.	

d

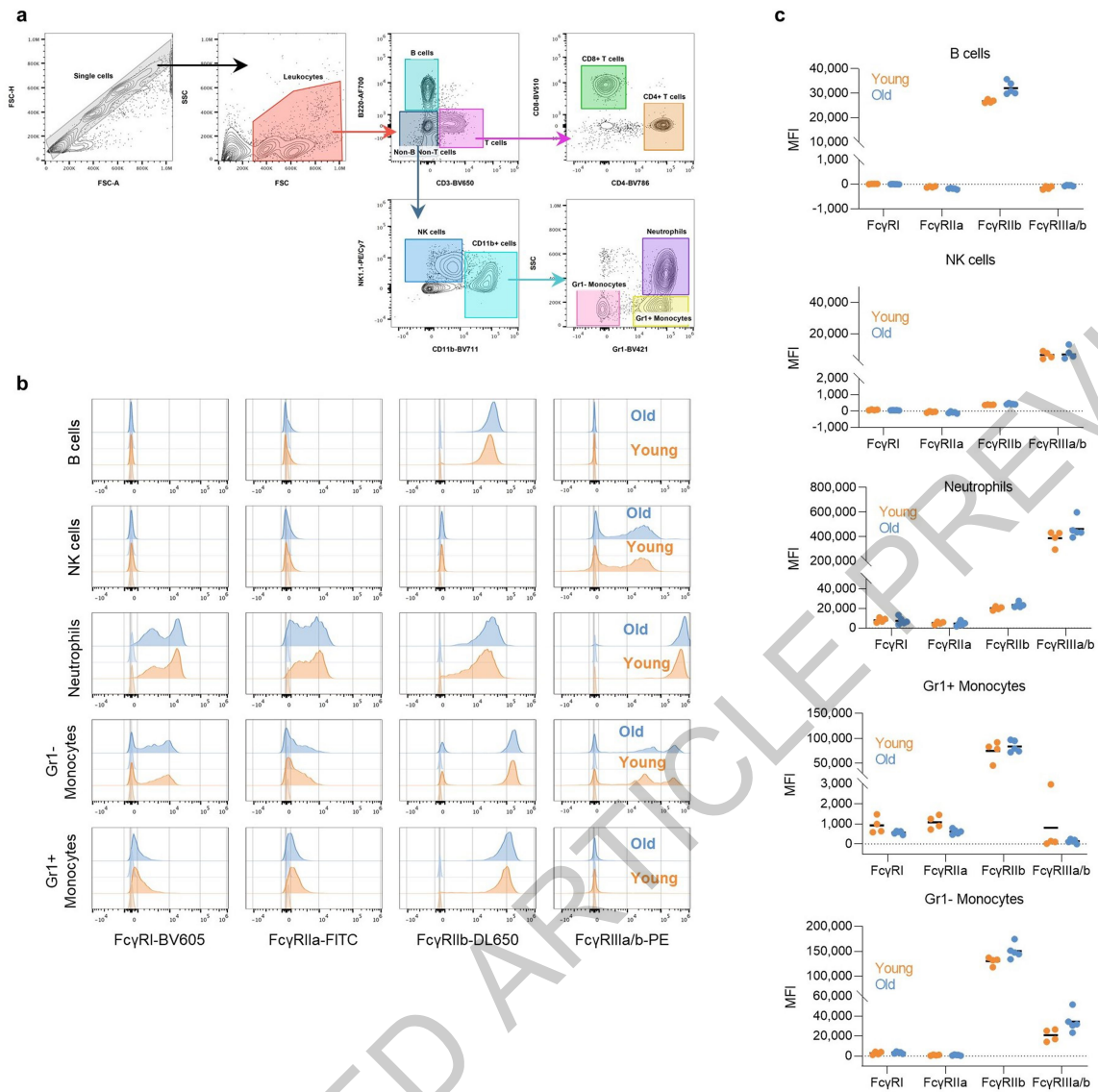
Hamster IgG	FcγRI		FcγRIIb		FcγRIII		FcγRIV	
	KD (M)	Fold	KD (M)	Fold	KD (M)	Fold	KD (M)	Fold
IgG1	$>1.0 \times 10^{-6}$	1.0	5.62×10^{-8}	1.0	3.55×10^{-8}	1.0	$>1.0 \times 10^{-6}$	1.0
IgG2	4.96×10^{-7}	>2	1.03×10^{-6}	0.05	7.02×10^{-7}	0.04	1.71×10^{-8}	> 58
IgG1-D265A	n.d.b.		n.d.b.		n.d.b.		n.d.b.	

e



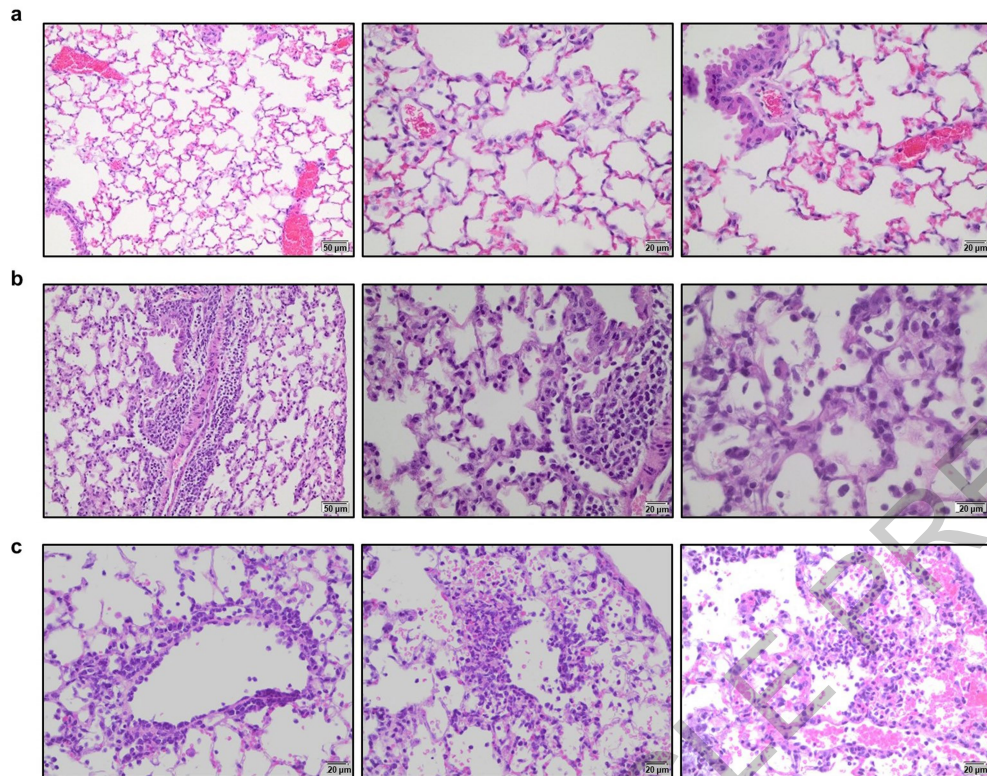
Extended Data Fig. 1 | Cloning and characterization of the IgG binding activity of hamster FcγRs. a, Syrian hamster FcγRs were cloned, and their sequences were determined. The FcγR ectodomains are underlined. b-e, The affinity of human IgG1 and Fc variants (b, e, SPR sensorgrams), as well as of

mouse (c) and hamster (d) IgG subclass variants for the various classes of hamster FcγRs was determined by surface plasmon resonance (SPR), using soluble hamster FcγR ectodomains. n.d.b., no detectable binding.



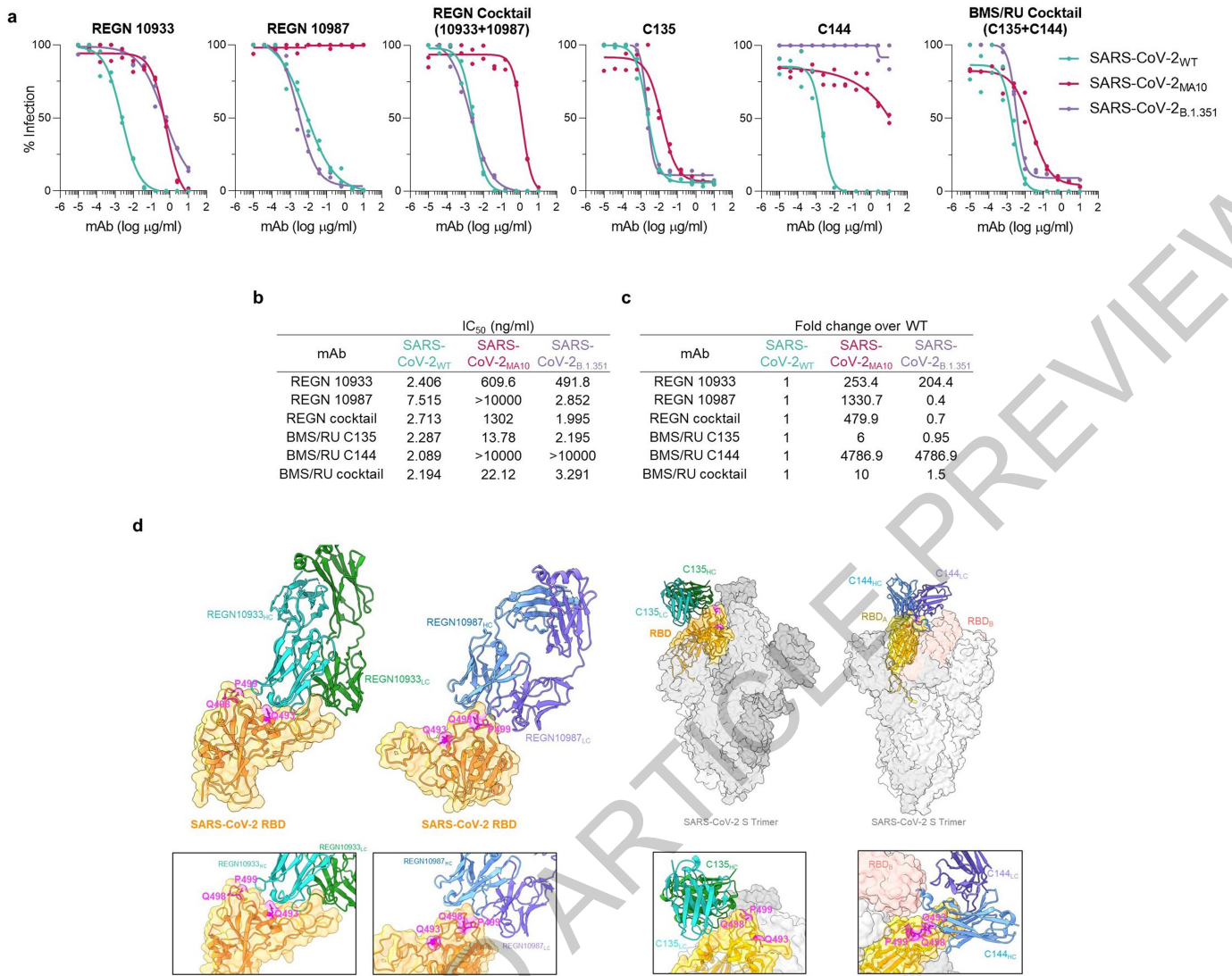
Extended Data Fig. 2 | Comparison of the Fc γ R expression levels in the various effector leukocyte populations between young and older Fc γ R humanized mice. Fc γ R expression was assessed by flow cytometry in peripheral blood leukocyte populations from young (6-7 weeks old; orange) and older (17 weeks old; blue) Fc γ R humanized mice. **a**, Gating strategy to identify the various leukocyte populations, **b**, Representative histogram

overlay plots of Fc γ R expression in young and older Fc γ R humanized mice. Corresponding isotype controls are indicated in lighter shade. **c**, Quantitation of Fc γ R expression (MFI, median fluorescence intensity subtracted from the respective isotype control) in various leukocyte populations. Results are from 4 or 5 mice per group for young and older mice, respectively.



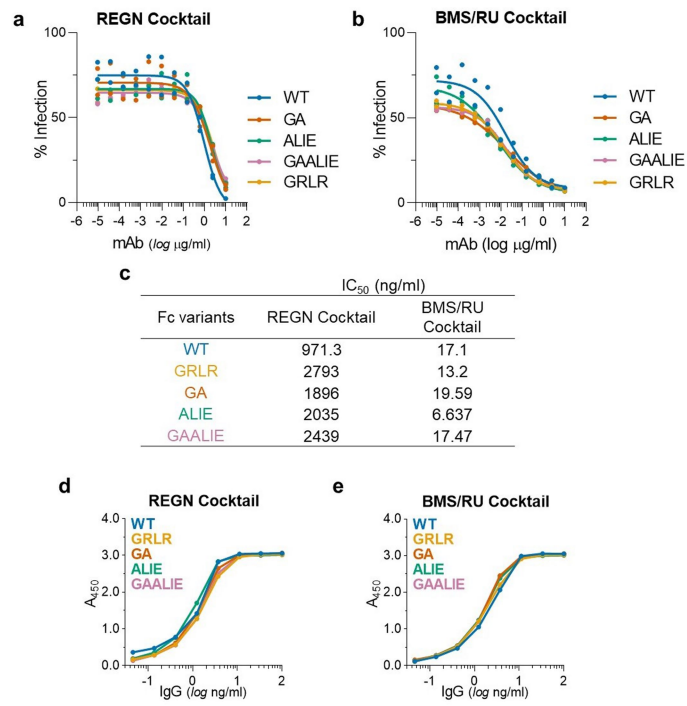
Extended Data Fig. 3 | Histopathological analysis of lung tissue from SARS-CoV-2-infected Fc γ R humanized mice. Lungs from SARS-CoV-2-infected (MA10 strain, 10^4 pfu, i.n.) Fc γ R humanized mice (16-22 weeks old) were harvested on day 4 post-infection and evaluated histologically to assess the pathological changes associated with SARS-CoV-2 infection. **a.** Uninfected mice were characterized by clear alveolar spaces and absence of inflammatory cell infiltrates (low magnification (left panel, 200x); high magnification (center and right panels, 400x)). **b.** In contrast, SARS-CoV-2 infection was associated with perivascular and peribronchial mononuclear leukocyte

infiltration (200x left; 400x center panel), as well as the presence of macrophages and neutrophils in alveoli and necrotic cellular debris in alveolar spaces (600x, right panel). **c.** In addition, SARS-CoV-2-infected mice exhibited perivenular mixed neutrophilic, histiocytic, and lymphocytic inflammation, reactive endothelium and extravasation of leukocytes (left panel, 400x), as well as foci of interstitial neutrophilic and macrophage inflammation with hemorrhage and single cell necrosis (center and right panels, 400x). Images are representative of one uninfected and six infected mice.

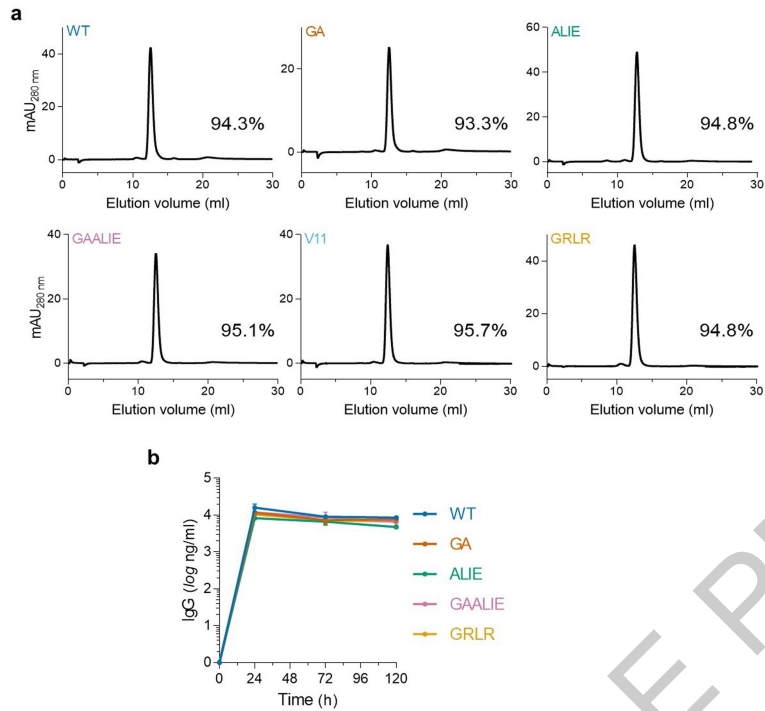


Extended Data Fig. 4 | In vitro neutralization activity of anti-SARS-CoV-2 mAbs against SARS-CoV-2 strains. Neutralization activity of REGN and BMS/RU mAbs (individual mAbs or as a cocktail) against SARS-CoV-2 pseudotyped reporter viruses was measured by *in vitro* neutralization assay. **(a)** *In vitro* neutralization curves and **(b)** IC₅₀ values of REGN (upper panel) and BMS/RU (lower panel) against SARS-CoV-2 WT, MA10, or B.1.351. **(c)** Fold change of

SARS-CoV-2_{MA10} and SARS-CoV-2_{B.1.351} IC₅₀ was calculated over WT. n=1 experiment performed in duplicates. **(d)** Cryo-EM structures of REGN10933 and REGN10987 complexed with SARS-CoV-2 (PDB: 6XDG) or C135 (PDB: 7K8Z) and C144 (PDB: 7K90) complexed with the SARS-CoV-2 spike trimer. Residues within the SARS-CoV-2_{WT} RBD that are mutated in the SARS-CoV-2_{MA10} strain (Q493K, Q498Y, P499T) are indicated in magenta.

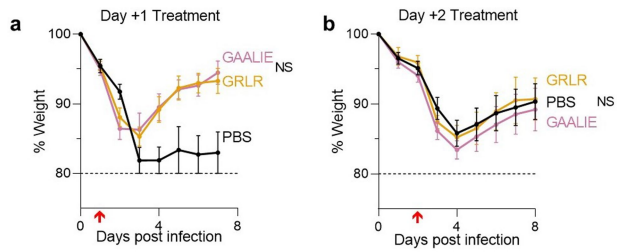


Extended Data Fig. 5 | *In vitro* neutralization activity and antigenic specificity of Fc variants of anti-SARS-CoV-2 mAbs. To confirm that changes in the Fc domain have no effect on the neutralization activity and Fab-mediated functions of anti-SARS-CoV-2 mAb, Fc domain variants were characterized in (a-c) *in vitro* neutralization assays using SARS-CoV-2_{MA10} pseudotyped reporter viruses and (d, e) in ELISA assays using SARS-CoV-2 RBD. n=1 experiment performed in duplicates. (a, d) REGN and (b, e) BMS/RU mAb cocktails were expressed as Fc variants and their *in vitro* neutralization activity (a, b, c, IC₅₀ values) and (d, e) antigenic specificity was compared among Fc variants.



Extended Data Fig. 6 | *In vitro* and *in vivo* stability of Fc variants of anti-SARS-CoV-2 mAbs. (a) Size-exclusion chromatography (SEC) analysis of Fc variants to determine aggregate formation among Fc domain variants. The SEC elution profiles and abundance (percentage) of monomeric IgG is indicated for the different Fc variants. (b) Fc variants of the REGN mAb cocktail

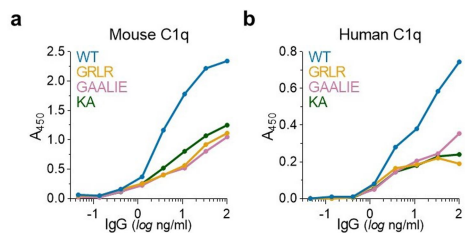
were administered (i.v.; 50 μ g) to Fc γ R humanized mice and antibody serum levels were determined by ELISA at various time points after antibody administration. n= total of 3 mice per group from two independent experiments. Data are mean \pm s.e.m.



Extended Data Fig. 7 | High-dose treatment of SARS-CoV-2-infected Fc γ R humanized mice with anti-SARS-CoV-2 mAbs Fc variants enhanced for activating Fc γ R binding is not associated with enhanced disease.

(a) Following the experimental strategy in Fig. 3b, SARS-CoV-2-infected (MA10, 10^4 pfu, i.n.) Fc γ R humanized mice (n=3 for PBS and n=5 for mAb-treated groups) were treated (i.v.) with 40 mg/kg REGN mAb cocktail expressed as Fc variants with diminished (GRLR) or enhanced activating Fc γ R binding (GAALIE). (b) SARS-CoV-2-infected mice were treated with 10 mg/kg BMS/RU mAb cocktail expressed as Fc variants GRLR or GAALIE on day 2 post infection. n= total of 10 mice per group for PBS, n=9 for GAALIE, and n=6 for GRLR from two independent experiments. Weight loss (mean \pm s.e.m.) was compared between GRLR and GAALIE-treated groups by two-way ANOVA (Bonferroni post hoc analysis adjusted for multiple comparisons). NS, not significant. Red arrow indicates time point of mAb treatment post-infection.

ACCELERATED ARTICLE PREVIEW



Extended Data Fig. 8 | Mouse and human C1q binding of Fc domain variants of IgG1. The capacity of IgG1 Fc domain variants to interact with mouse (a) and human (b) C1q was assessed by ELISA (n=1 experiment performed in duplicates). The KA (K322A) variant, which has previously described as a complement-deficient mutant²⁸, was included as control.

ACCELERATED ARTICLE PREVIEW

Reporting Summary

Nature Research wishes to improve the reproducibility of the work that we publish. This form provides structure for consistency and transparency in reporting. For further information on Nature Research policies, see our [Editorial Policies](#) and the [Editorial Policy Checklist](#).

Statistics

For all statistical analyses, confirm that the following items are present in the figure legend, table legend, main text, or Methods section.

n/a Confirmed

- | | | |
|-------------------------------------|-------------------------------------|--|
| <input type="checkbox"/> | <input checked="" type="checkbox"/> | The exact sample size (n) for each experimental group/condition, given as a discrete number and unit of measurement |
| <input type="checkbox"/> | <input checked="" type="checkbox"/> | A statement on whether measurements were taken from distinct samples or whether the same sample was measured repeatedly |
| <input type="checkbox"/> | <input checked="" type="checkbox"/> | The statistical test(s) used AND whether they are one- or two-sided
<i>Only common tests should be described solely by name; describe more complex techniques in the Methods section.</i> |
| <input type="checkbox"/> | <input checked="" type="checkbox"/> | A description of all covariates tested |
| <input type="checkbox"/> | <input checked="" type="checkbox"/> | A description of any assumptions or corrections, such as tests of normality and adjustment for multiple comparisons |
| <input type="checkbox"/> | <input checked="" type="checkbox"/> | A full description of the statistical parameters including central tendency (e.g. means) or other basic estimates (e.g. regression coefficient) AND variation (e.g. standard deviation) or associated estimates of uncertainty (e.g. confidence intervals) |
| <input type="checkbox"/> | <input checked="" type="checkbox"/> | For null hypothesis testing, the test statistic (e.g. F , t , r) with confidence intervals, effect sizes, degrees of freedom and P value noted
<i>Give P values as exact values whenever suitable.</i> |
| <input checked="" type="checkbox"/> | <input type="checkbox"/> | For Bayesian analysis, information on the choice of priors and Markov chain Monte Carlo settings |
| <input checked="" type="checkbox"/> | <input type="checkbox"/> | For hierarchical and complex designs, identification of the appropriate level for tests and full reporting of outcomes |
| <input checked="" type="checkbox"/> | <input type="checkbox"/> | Estimates of effect sizes (e.g. Cohen's d , Pearson's r), indicating how they were calculated |

Our web collection on [statistics for biologists](#) contains articles on many of the points above.

Software and code

Policy information about [availability of computer code](#)

Data collection GE Unicorn v6.3, SoftMaxPro v7.0.2, Biacore T200 control software v2.0, Attune NxT flow cytometry software v3.1.2, Microsoft Excel, Applied Biosystems QuantStudio 6 Flex Real-Time PCR, software v1.3, Olympus BX45 light microscope with an SC30 camera, Illumina MiSeq

Data analysis GE Unicorn v6.3, SoftMaxPro v7.0.2, Biacore T200 evaluation software v2.0, QuantStudio Real-Time PCR Software v1.3, Graphpad Prism v9, Microsoft Excel v2008, SeqBuilder Pro v16 and v17, SeqMan Pro v16 and v17, Olympus cellSens Dimension software, FlowJo v10.7.

For manuscripts utilizing custom algorithms or software that are central to the research but not yet described in published literature, software must be made available to editors and reviewers. We strongly encourage code deposition in a community repository (e.g. GitHub). See the Nature Research [guidelines for submitting code & software](#) for further information.

Data

Policy information about [availability of data](#)

All manuscripts must include a [data availability statement](#). This statement should provide the following information, where applicable:

- Accession codes, unique identifiers, or web links for publicly available datasets
- A list of figures that have associated raw data
- A description of any restrictions on data availability

Raw data for all main and extended data figures are included in the manuscript as source files.

Field-specific reporting

Please select the one below that is the best fit for your research. If you are not sure, read the appropriate sections before making your selection.

- Life sciences Behavioural & social sciences Ecological, evolutionary & environmental sciences

For a reference copy of the document with all sections, see [nature.com/documents/nr-reporting-summary-flat.pdf](https://www.nature.com/documents/nr-reporting-summary-flat.pdf)

Life sciences study design

All studies must disclose on these points even when the disclosure is negative.

Sample size	No statistical method was used to predetermine sample size. For in vivo experiments, based on preliminary studies that determined experimental variation in survival following infection and mAb treatment, we have performed power calculations and determined that at least n=6 mice/group is sufficient to detect differences among experimental groups (powered at 80% for 5% significance level; survival assessed by log-rank (Mantel-Cox) test). For in vitro experiments, assays were performed using the indicated sample sizes to ensure reproducibility.
Data exclusions	No data were excluded.
Replication	The reported findings have been confirmed in large groups of mice/experimental group in multiple (>2) experiments. The enhanced protective activity of the Fc engineered variants was confirmed in multiple experiments using a variety of mAbs that target different epitopes on SARS-CoV-2 Spike protein. Also, two different challenge virus strains have been used (NY isolate and MA10) in two different animal models (hamsters and mice, respectively) to minimize strain-specific effects.
Randomization	Mice were randomized based on age, gender, and weight. Prior to treatment, we ensured that the mean weight and age were comparable among the various treatment groups. No randomization was used for the in vitro experiments, as it is not applicable to the study design. In vitro experiments did not involve experimental groups with different treatment conditions.
Blinding	Blinding is not relevant for this study, as this is an observational (not case-control) study.

Reporting for specific materials, systems and methods

We require information from authors about some types of materials, experimental systems and methods used in many studies. Here, indicate whether each material, system or method listed is relevant to your study. If you are not sure if a list item applies to your research, read the appropriate section before selecting a response.

Materials & experimental systems

n/a	Involvement in the study
<input type="checkbox"/>	<input checked="" type="checkbox"/> Antibodies
<input type="checkbox"/>	<input checked="" type="checkbox"/> Eukaryotic cell lines
<input checked="" type="checkbox"/>	<input type="checkbox"/> Palaeontology and archaeology
<input type="checkbox"/>	<input checked="" type="checkbox"/> Animals and other organisms
<input checked="" type="checkbox"/>	<input type="checkbox"/> Human research participants
<input checked="" type="checkbox"/>	<input type="checkbox"/> Clinical data
<input checked="" type="checkbox"/>	<input type="checkbox"/> Dual use research of concern

Methods

n/a	Involvement in the study
<input checked="" type="checkbox"/>	<input type="checkbox"/> ChIP-seq
<input type="checkbox"/>	<input checked="" type="checkbox"/> Flow cytometry
<input checked="" type="checkbox"/>	<input type="checkbox"/> MRI-based neuroimaging

Antibodies

Antibodies used

The clones of the recombinant anti-SARS-CoV-2 antibodies are reported in the manuscript and their characteristics are also described in previously published studies (relevant citations included in the manuscript).

For ELISA assays, the following antibodies were used: HRP-conjugated goat F(ab')₂ anti-human IgG (H+L)(Jackson ImmunoResearch, 109-036-088, Lot: 147433, 1:5000); Biotin-conjugated goat F(ab')₂ anti-human IgG (F(ab')₂-specific)(Jackson ImmunoResearch, 109-066-088, Lot: 139987 5 µg/ml); Mouse anti-C1q antibody (Abcam, ab71940).

The following antibodies were used for flow cytometry (unless otherwise noted, all antibodies were used at 1:200 dilution): anti-B220-AF700 (Biolegend, 103232, RA3-6B2, B272460); anti-Gr-1-BV421 (Biolegend, 108445, RB6-8C5, B292607); anti-CD8b-BV510 (Biolegend, 126631, YTS156.7.7, B303593); anti-CD3-BV650 (Biolegend, 100229, 17A2, B282105, used at 1:100 dilution); anti-CD11b-BV711 (Biolegend, 101242, M1/70, B315411); anti-CD4-BV785 (Biolegend, 100453, GK1.5, B284013); anti-NK1.1-PE/Cy7 (Invitrogen, 25-5941-82, PK136, 1981963); anti-human FcγRI-BV605 (Biolegend, 305034, 10.1, B293272); anti-human FcγRIIIa-FITC (Stemcell technologies, 60012FI, IV.3)

anti-human FcγRIIb-Dylight650; (clone 2B6, produced in house and conjugated with Dylight650 kit)
 anti-human FcγRIIIa/b-PE (Biolegend, 980102, 3G8, B301142)
 Mouse IgG1 isotype control-Dylight650 (ThermoFisher, MA1-191-D650, MOPC-21)
 Mouse IgG2b kappa isotype control - FITC (ThermoFisher, 11-4732-42, eBMG2b)
 Mouse IgG1 kappa isotype control-PE (Biolegend, 400112, MOPC-21, B291605)
 Mouse IgG1 kappa isotype control-BV605 (Biolegend, 400162, MOPC-21, B329915)
 anti-human FcγRI (Biolegend, 305048, 10.1, B303217)
 anti-human FcγRIIIa (Stemcell technologies, 60012, IV.3)
 anti-human FcγRIIb (clone 2B6, produced in house)
 anti-human FcγRIIIa/b (Biolegend, 302049, 3G8)

Validation

For recombinant anti-SARS-CoV-2 mAbs, their antigenic specificity and neutralization activity were assessed in in vitro assays (data presented in the manuscript Extended Data Figure 5) to ensure that changes in the Fc domain have no impact on their Fab-mediated activities. Purity of recombinant proteins was assessed by SDS-PAGE followed by SafeStain blue staining (ThermoFisher) and SEC. All antibody preparations were >94% pure and endotoxin levels were <0.05 EU/mg, as determined by the Limulus Amebocyte Lysate (LAL) assay.

For commercially available antibodies, validation has been performed by the manufacturer and corresponding certificates of analysis are available at the manufacturer's website. Specificity is tested in 1-3 target cell types with either single- or multi-color analysis (including positive and negative cell types). Once specificity is confirmed, each new lot is validated to ensure that it performs with similar intensity to the in-date reference lot. Brightness (MFI) is evaluated from both positive and negative populations. Each lot product is validated by QC testing with a series of titration dilutions.

The specificity of antibodies used for ELISA were validated by the manufacturer by immunoelectrophoresis and/or ELISA. No reactivity was detected against non-immunoglobulin serum proteins. Antibodies are also tested by the manufacturer by ELISA and/or solid-phase adsorbed to ensure minimal cross-reaction with immunoglobulins from other species.

Eukaryotic cell lines

Policy information about [cell lines](#)

Cell line source(s)

VeroE6, Caco-2, 293T - ATCC
 Expi293F - ThermoFisher
 Huh7.5 - Charles Rice laboratory, Rockefeller University
 HT1080-ACE2 - Paul Bieniasz laboratory, Rockefeller University

Authentication

Cell lines were not authenticated after purchase

Mycoplasma contamination

All cell lines have been tested by the manufacturer and were tested negative for mycoplasma contamination. Certificates of analysis are available in manufacturer's website. All cell lines were maintained for <10 passages to minimize mycoplasma contamination. Media and supplements (FBS) were also all mycoplasma-free (per certificate of analysis).

Commonly misidentified lines
(See [ICLAC](#) register)

No commonly misidentified cell lines were used in this study.

Animals and other organisms

Policy information about [studies involving animals](#); [ARRIVE guidelines](#) recommended for reporting animal research

Laboratory animals

Syrian golden hamsters (strain code 049) were purchased from Charles River laboratories. Males, 6-8 wk old hamsters were used. FcγR knockout (mFcγRα^{-/-}; Fcgr1^{-/-}) and FcγR humanized mice (mFcγRα^{-/-}, Fcgr1^{-/-}, hFcγRI⁺, hFcγRIIIaR131⁺, hFcγRIIb⁺, hFcγRIIIaF158⁺, and hFcγRIIIb⁺) were generated in the C57BL/6 background and characterized in previous studies. Males or females; 6-7 or 16-22 weeks old mice were used in this study. Hamsters and mice were housed at a controlled ambient temperature (20-25oC) and humidity (30-70%) environment with 12-hour light/dark cycle.

Wild animals

No wild animals were used in this study.

Field-collected samples

No field-collected samples were used in this study.

Ethics oversight

All in vivo experiments were performed in compliance with federal laws and institutional guidelines and have been approved by the Rockefeller University Institutional Animal Care and Use Committee. In-vivo experiments in hamsters were also in compliance with USDA regulations.

Note that full information on the approval of the study protocol must also be provided in the manuscript.

Plots

Confirm that:

- The axis labels state the marker and fluorochrome used (e.g. CD4-FITC).
- The axis scales are clearly visible. Include numbers along axes only for bottom left plot of group (a 'group' is an analysis of identical markers).
- All plots are contour plots with outliers or pseudocolor plots.
- A numerical value for number of cells or percentage (with statistics) is provided.

Methodology

Sample preparation

Mouse blood was collected from the retro-orbital venous plexus. Following RBC lysis (RBC lysis buffer; Biolegend), single cell suspensions were resuspended in PBS containing 0.5% (w/v) BSA and 5 mM EDTA. Cells were labeled with mixtures of fluorescently labeled antibodies incubated at 4C for 15 min and washed twice with PBS containing 0.5% (w/v) BSA and 5 mM EDTA prior to analysis.

Instrument

0A29009 Attune NxT Acoustic Focusing Cytometer (Lasers: BRV6Y)

Software

For data acquisition, Attune NxT flow cytometry software v3.1.2 was used. For data analysis, FlowJo v10.7 was used.

Cell population abundance

No sorting performed

Gating strategy

The gating strategy is presented in Extended Data Figure 2. Single cells were identified in FSC-A vs. FSC-H plots. For analysis of FcR expression on mouse blood cells, single cell leukocytes (identified based on FSC-A vs. FSC-H and SSC-A vs. FSC-A plots) are gated as B220 vs. CD3 to identify B220+ and CD3+ cells. CD3+ events are plotted as CD8 vs. CD4 to identify CD8 (CD8+/CD4-) and CD4 (CD4+/CD8-) T cells. B220-/CD3- cells are plotted as NK1.1 vs. CD11b to identify NK cells (gated as NK1.1+) and CD11b+ cells. CD11b+ were further plotted as SSC vs. Gr1. Neutrophils are identified as CD11b+/SSC+/Gr1+ cells. Gr1- monocytes are identified as CD11b+/SSC-/Gr1- cells. Gr1+ monocytes are identified as CD11b+/SSC-/Gr1+ cells.

- Tick this box to confirm that a figure exemplifying the gating strategy is provided in the Supplementary Information.